



Title	Micro-milling super-fine powdered activated carbon decreases adsorption capacity by introducing oxygen/hydrogen-containing functional groups on carbon surface from water
Author(s)	Takaesu, Hideki; Matsui, Yoshihiko; Nishimura, Yuki; Matsushita, Taku; Shirasaki, Nobutaka
Citation	Water Research, 155, 66-75 https://doi.org/10.1016/j.watres.2019.02.019
Issue Date	2019-05-15
Doc URL	http://hdl.handle.net/2115/81364
Rights	©2019. This manuscript version is made available under the CC-BY-NC-ND 4.0 license http://creativecommons.org/licenses/by-nc-nd/4.0/
Rights(URL)	http://creativecommons.org/licenses/by-nc-nd/4.0/
Type	article (author version)
File Information	02_MicromillingSuperfine.pdf



[Instructions for use](#)

1
2
3
4
5
6
7
8
9
10
11
12
13
14
15
16
17
18
19
20
21

Micro-milling Super-fine Powdered Activated Carbon Decreases Adsorption Capacity by Introducing Oxygen/hydrogen-Containing Functional Groups on Carbon Surface from Water

Hideki Takaesu¹, Yoshihiko Matsui^{2,*}, Yuki Nishimura¹, Taku Matsushita², and Nobutaka Shirasaki²

¹Graduate School of Engineering, Hokkaido University

²Faculty of Engineering, Hokkaido University

* Corresponding author. Phone: +81-11-706-7280.

E-mail address: matsui@eng.hokudai.ac.jp

Address: North13, West 8, Sapporo 060-8628, Japan

22 **Abstract**

23

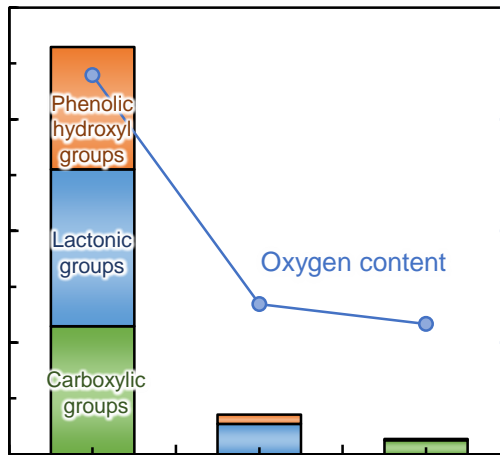
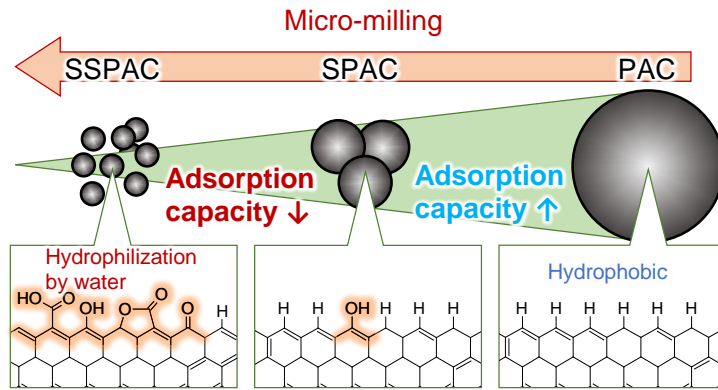
24 Superfine powdered activated carbon (SPAC) of micron to submicron particle size is
25 produced by micro-milling of conventionally sized powdered activated carbon. SPAC has
26 attracted attention because of its high adsorption capacity; however, milling to the
27 submicron particle size range lowers its adsorption capacity. Here, we found that this
28 decrease of adsorption capacity was due to the introduction of oxygen/hydrogen-
29 containing functional groups into the graphene structure of the carbon from water during
30 the milling, causing it to become less hydrophobic. This finding was supported by three
31 analyses of SPAC particles before and after milling: 1) elemental analysis revealed
32 increased oxygen and hydrogen content, 2) Boehm titration analysis revealed increased
33 amounts of acidic functional groups, including carboxylic and phenolic hydroxyl groups,
34 and 3) Fourier-transform infrared spectroscopy showed increased peaks at 1200, 1580, and
35 3400 cm^{-1} , confirming the presence of those groups. Dissolved oxygen concentration did
36 not strongly affect the increase of oxygen content in SPAC, and no evidence was found for
37 hydroxyl radical production during micro-milling, suggesting that a mechanochemical
38 reaction underlies the increase in oxygen/hydrogen-containing functional groups. An
39 increase in ^{18}O content in the SPAC particles after milling in water- ^{18}O indicated that the
40 oxygen in the functional groups originated from the surrounding water.

41

42

43 **Key words:** SPAC; Geosmin; Bentazone; Isotherm; Mechanochemical reaction

44



45

46

47 **1. Introduction**

48

49 Superfine powdered activated carbon (SPAC) has attracted attention for its high adsorption
50 capacity and kinetics (Amaral et al. 2016, Ando et al. 2010, Bonvin et al. 2016, Dunn and
51 Knappe 2013, Heijman et al. 2009, Jiang et al. 2015, Matsui et al. 2004, Matsui et al. 2015,
52 Matsui et al. 2012). In full-scale water treatment plants, SPAC with a particle diameter of
53 1 to 3 μm , produced onsite from conventional-size powdered activated carbon (PAC), is
54 currently used as an adsorbent during pretreatment before membrane filtration (Kanaya et
55 al. 2015). Micro-milling technology is now able to produce submicron SPAC (SSPAC)
56 with a particle diameter down to 140 nm (Ellerie et al. 2013, Pan et al. 2017a, Partlan et
57 al. 2016). However, it has been shown that micro-milling increases the oxygen content of
58 activated carbon (AC) (Partlan et al. 2016) and decreases its capacity to adsorb 2-
59 methylisoborneol (MIB) (Pan et al. 2017a), although the internal pore volume and surface
60 area of AC particles are not substantially changed (Pan et al. 2017b, Partlan et al. 2016).
61 Similarly, it has also been reported that ball-milling has no effect on the structure of AC
62 particles (Welham and Williams 1998).

63

64 AC with a low oxygen content has a greater capacity than AC with a high oxygen content
65 for adsorption of hydrophobic micro-pollutants such as MIB (Considine et al. 2001,
66 Pendleton et al. 1997). Oxygen can form various oxygen-containing functional groups,
67 such as carboxyl, carbonyl and phenolic hydroxyl functional groups, on the AC particle
68 surface, which promote the formation of water clusters at the particle surface that impede,
69 or prevent, the adsorption of hydrophobic micro-pollutants (Pendleton et al. 2002,
70 Quinlivan et al. 2005).

71

72 Thus, it can be hypothesized that micro-milling promotes the formation of oxygen-
73 containing functional groups at the AC particle surface, causing the oxygen content of the
74 AC to increase and its adsorption capacity to decrease; this hypothesis, and the underlying
75 mechanism, have yet to be confirmed, although the underlying mechanism may involve a
76 mechanochemical reaction (Balaz et al. 2013). Micro-milling AC particles and the changes
77 of the characteristics of AC particles induced by micro-milling are important issues for
78 optimizing SPAC for the efficient removal of micro-pollutants from water (Partlan et al.
79 2016).

80

81 Here, we clarified that the amount of oxygen/hydrogen-containing functional groups on
82 the surface of AC particles is increased by micro-milling and investigated the causes of
83 this increase. Three environmentally relevant micro-pollutants were selected as target
84 adsorbates (WHO 2011): MIB, geosmin, and bentazone. MIB and geosmin are
85 cyanobacterial metabolites that influence the quality of drinking water due to their strong,
86 earthy or musty taste and odor with a very low odor detection threshold. These compounds
87 can be removed from water by adsorption onto AC because of their hydrophobicity (log
88 Kow value, 3.31 and 3.57, respectively), although the amount removed is variable.
89 Bentazone is a pesticide that because of its high hydrophilicity (log Kow value, -0.46) is
90 not readily adsorbed by AC.

91

92

93 **2. Experimental**

94

95 ***2.1 Activated carbons***

96

97 Three wood-based PACs (W-TK, W-TKO and W-SR) and two coconut-based PACs (C-
98 TK and C-SR) with median diameters (D50s) of 4–24 μm were obtained from Futamura
99 Chemical Co., Tokyo, Japan (W-TK, W-TKO and C-TK) and Osaka Chemical Co., Osaka,
100 Japan (W-SR and C-SR). Large SPAC (SPAC_L; D50, 2.3–5.1 μm) was produced by wet-
101 milling these PACs with a ball mill (Nikkato, Osaka, Japan). Small SPAC (SPAC_S, 0.9–
102 1.4 μm) and SSPAC (0.13–0.23 μm) were produced with a bead mill (LMZ015, Ashizawa
103 Finetech, Chiba, Japan). Details of the milling procedures are as follows.

104

105 *Normal milling procedure:* SPAC_L was obtained by ball-milling PACs slurry (15% w/w)
106 at 45 rpm for 4–5 h. After diluting the SPAC_L slurry with pure water to approximately 1%
107 (w/w), the SPAC_L was bead-milled with ZrO₂ beads (ϕ 0.3 mm) at a speed of 8 m/s (2590
108 rpm) for 20–30 min and SPAC_S was obtained. SSPAC were obtained by bead-milling
109 SPAC_L using ZrO₂ beads (ϕ 0.1 mm) at 12 m/s (3884 rpm) unless otherwise specified for
110 1.5–6 h. A cooling system kept the temperature of the slurry below 28°C during bead-
111 milling.

112

113 *Anoxic milling procedure:* After drying PAC in a vacuum chamber for > 1 h, the PAC was
114 rinsed with pure water three times in a glove box filled with nitrogen gas. After preparing
115 the PAC slurry of 15% (w/w), the PAC slurry was transferred to the ball mill in the glove
116 box. SPAC_L slurry was obtained by ball-milling the PAC slurry. The SPAC_L slurry
117 concentration was adjusted to about 1% (w/w), and then the DO of the slurry was removed
118 to < 1 mg/L by purging with nitrogen gas. SPAC_S and SSPAC were obtained by bead
119 milling the SPAC_L slurry under nitrogen gas purging. The other conditions of the anoxic
120 milling were the same as those of the normal milling.

121

122 **2.2 AC characterization**

123

124 2.2.1 Particle size

125

126 AC slurries (50 mL) were supplemented with dispersant (0.08% w/v, Triton X-100, Kanto
127 Chemical, Tokyo, Japan), and then they were ultra-sonicated (150 W, 19.5 kHz) for 6 min
128 (SSPAC) or 1 min (PAC, SPAC_L and SPAC_S). Particle sizes of the ACs were determined
129 by a Microtrac analyzer (MT3300EXII, Nikkiso, Tokyo, Japan) (Pan et al. 2017a).

130

131 2.2.2 Elemental analysis

132

133 Elemental compositions (H, C, N, O and S) of ACs were determined according to the
134 procedure of Pan et al. (2017a). In brief, after drying AC slurries under vacuum at ~20 °C,
135 the ACs were packed in silver capsules, and then the capsules were weighed. After the
136 capsules were placed under vacuum, they were transferred to a CHNS/O elemental
137 analyzer (Vario EL Cube, Elementar Japan, Yokohama, Japan) to measure the elemental
138 contents. Triplicate measurements were conducted for each AC sample to give the average.

139

140 2.2.3 Boehm titration method

141

142 Boehm titration (Biniak et al. 1997, Noh and Schwarz 1990) was applied to determine the
143 surface functional groups of the ACs. AC slurry containing 200 mg of AC in a glass test
144 tube was supplemented with 0.1 N NaOH, Na₂CO₃, NaHCO₃, or HCl solution of the same
145 volume as the AC slurry. The resulting slurry was placed under a vacuum and then under

146 a N₂ atmosphere. After sealing the tube containing the slurry, the tube was shaken at 20
147 °C for 2 days. After centrifugation (4000 rpm, 2764g) of the slurry, the supernatant was
148 filtered through a hydrophilic polytetrafluoroethylene membrane (0.2-μm pore size, Toyo
149 Roshi Kaisha, Tokyo, Japan). The filtrate (10 mL) was mixed with a HCl (0.05 N, 20 mL)
150 or NaOH (0.05 N, 20mL) solution. After the mixture was sparged with N₂ gas for 45–60
151 min, it was back-titrated with a NaOH or HCl solution to quantify the uptake of one of the
152 bases (NaOH or Na₂CO₃, NaHCO₃) or the acid (HCl). By assuming that NaHCO₃
153 neutralized carboxylic groups only, Na₂CO₃ neutralized carboxylic and lactonic groups,
154 and NaOH neutralized all acidic groups including the phenolic hydroxyl group (Boehm
155 1966, Boehm 2002), the differences between the uptakes of the bases was used to estimate
156 the amount of sites with one specific acid group (carboxylic, lactonic, or phenolic hydroxyl
157 group). The amount of basic sites was calculated from the amount of HCl required in the
158 titration. All chemicals used were reagent grade (Wako Pure Chemical Industries, Osaka,
159 Japan).

160

161 2.2.4 Fourier-transform infrared spectroscopy

162

163 AC slurries were dried under vacuum at ~ 20 °C to avoid oxidation during drying. The
164 dried samples were mixed with KBr at 1:500 mass ratio. The mixture was compacted into
165 a pellet, and the pellet was kept under vacuum before transmission measurement. The
166 transmission measurement was conducted with a Fourier-transform infrared spectroscopy
167 (FTIR) spectrometer (FTIR-8400S, Shimadzu, Kyoto, Japan).

168

169 2.2.5 Production of SSPAC in water-¹⁸O and isotope analysis

170

171 After rinsing with pure water three times, the slurry of PAC was ball-milled by the normal
172 milling procedure to produce SPAC_L slurry. SPAC_L slurry (500 mL) was supplemented
173 with 3 mL of ¹⁸O-enriched water (10 at.%, Taiyo Nippon Sanso, Tokyo, Japan). The
174 supplemented slurry was then bead-milled under the anoxic condition for 2–6 h at 12 m/s
175 with ϕ 0.1-mm beads to produce SSPAC. The AC slurries were dried under vacuum at
176 ~20 °C and then capsuled for isotope ratio analysis. Capsulation in a glovebox filled with
177 nitrogen gas was also conducted. Isotope ratio analysis was conducted to determine the
178 isotopic composition of the samples by using an ANCA-GSL elemental analyzer (Sercon,
179 Cheshire, UK) in the analytical laboratory (Kyoto, Japan) of Taiyo Nippon Sanso. $\delta^{18}\text{O}$
180 values were calculated from the ¹⁸O/¹⁶O ratios.

181

182 A control experiment was conducted in which a portion (10 mL) of SSPAC produced by
183 2- or 6-hour bead-milling under the anoxic condition was supplemented with 0.056 mL
184 of ¹⁸O-enriched water (10 at.%) and mixed with no milling for 2–6 h. The AC slurry was
185 then dried under vacuum at ~20°C and capsuled for isotope ratio analysis.

186

187 *2.3 Adsorption experiments*

188

189 The working solutions of MIB, geosmin, and bentazone were prepared by adding each
190 reagent-grade chemical (Wako Pure Chemical Industries) to organic-free ionic water: the
191 ion composition was the same as those used in previous researches (Matsui et al. 2015, Pan
192 et al. 2016). Batch adsorption isotherm tests were conducted by the bottle-point technique
193 (Pan et al. 2017a). Different amounts of AC were added to 110-mL vials containing the
194 working solutions. Immediately after the AC addition, the vials were shaken on a rotary
195 shaker at 20°C in the dark (Matsui et al. 2013, Matsui et al. 2012). After shaking for 1

196 week for PAC and SPAC_L or 3 days for SPAC_S and SSPAC, the AC particles were
197 separated by filtering the solution through a hydrophilic polytetrafluoroethylene membrane,
198 and the liquid-phase adsorbate concentrations were measured. Adsorbate concentrations in
199 solid phase were calculated from mass balances.

200

201 MIB concentrations were determined by purge and trap gas chromatography/mass
202 spectrometry (Aqua PT 5000 J, GL Sciences, Tokyo, Japan; GCMS-QP2010 Plus,
203 Shimadzu, Kyoto, Japan) or headspace–solid-phase microextraction gas
204 chromatography/mass spectrometry (PAL RSI 85; 7820A/5977 E MSD, Agilent Agilent
205 Technologies Japan) according to the procedure of Pan et al. (2017a). Geosmin
206 concentration was determined by methods similar to those used for MIB. The bentazone
207 concentration was determined by liquid chromatography/Orbitrap mass spectrometry (Q
208 Exactive; UltiMate3000 LC systems, Thermo Fisher Scientific, Tokyo, Japan) using a
209 Hypersil GOLD column (1.9 μm, 50 mm × 2.1 mm), a temperature of 40°C, a mobile phase
210 (methanol:2 mM formic acid = 70:30), and flow rate of 0.2 mL/min; *m/z* 239.0496 was
211 attributed to bentazone.

212

213

214 **3. Results and Discussion**

215

216 ***3.1 Adsorption capacity***

217

218 Adsorption isotherms of MIB, geosmin, and bentazone on the wood-based and coconut-
219 based ACs of different particle sizes were obtained to observe how adsorption capacity
220 was changed by milling. The adsorption isotherms were changed with milling. Changes of

221 isotherms with particle size are depicted in Figures 1S–4S. Because the slopes in the plot
222 of $\log-q$ vs. $\log-c$ plot were almost the same, where q and c denote solid-phase and liquid-
223 phase concentrations, respectively, the adsorption capacity of each AC for each adsorbate
224 was then represented by the solid-phase concentration at a specific liquid-phase
225 concentration, after describing the isotherm data by the Freundlich equation.

226

227 For MIB adsorption on the various ACs, we confirmed the trend reported by Pan et al.
228 (2017a), who observed that the MIB adsorption capacity of a wood-based AC increased
229 with decreasing particle diameter from 10 to 1 μm , but decreased with decreasing particle
230 diameter from 1 to 0.2 μm (Figure 1). In the present study, the changes in adsorption
231 capacity for geosmin were more prominent than those for MIB. In addition to the changes
232 observed for the hydrophobic compounds MIB and geosmin, a similar trend was observed
233 for the highly hydrophilic compound bentazone. Pan et al. (2017a) attributed the decrease
234 of adsorption capacity with decreasing particle size in the submicron-diameter range to the
235 AC oxidation during micro-milling, and the increase of adsorption capacity in the 10- μm
236 diameter range to adsorption on the external particle surface, and they presented a
237 correlation between adsorption capacity and oxygen content of AC particles with diameters
238 less than 2 μm (PAC_s and SSPAC). For such small-size AC, adsorption occurs both
239 internally and externally, suggesting that pore surface chemistry, as represented by oxygen
240 content, strongly affects adsorption capacity. To assess the adsorption of geosmin,
241 bentazone, and MIB on the different ACs, we examined the correlations between
242 adsorption capacities and oxygen content (Figure 2) and verified that the reduction of
243 adsorption capacity during micro-milling was related to the increase of the oxygen content
244 of the AC particles.

245

246 *3.2 Changes in the amounts of oxygen-containing functional groups and elemental*
247 *composition*

248

249 The results of the elemental analysis are shown in Figures 3 and 5S. The oxygen content
250 of the ACs increased with decreasing particle size, which is in accordance with the results
251 of previous studies (Dunn and Knappe 2013, Partlan et al. 2016). In our study, the diameter
252 of AC particles did not change substantially after the median diameter reached around 150
253 nm. Thus, this diameter was considered to be the minimum critical median particle
254 diameter (equilibrium state) of our micro-milling system. However, the oxygen content of
255 the ACs continued to increase with increasing milling time, even after the equilibrium state
256 had been reached. The equilibrium state of milling is related not only to
257 aggregation/agglomeration, but also to fracture, of the AC particles (Balaz et al. 2013,
258 Berndt 2004). Thus, our data suggest that although particle size remained unchanged once
259 the equilibrium state was reached, the AC particles were fractured, and new particle
260 surfaces were generated with continued milling.

261

262 A similar trend was observed for hydrogen (Figures 3 and 5S). The hydrogen content of
263 the ACs increased with milling, although the total hydrogen content remained small. The
264 increase in hydrogen content is briefly noted by Pan et al. (2017a), but the supporting data
265 is limited. Our data clearly showed that the increase in hydrogen content was in proportion
266 to the increase in oxygen content (Figure 3, lower right panel, and Figure 5S). In contrast,
267 the carbon content of the ACs decreased, and the nitrogen and sulfate content remained
268 small and unchanged.

269

270 According to our Boehm titration observations, the amount of acidic functional groups
271 increased with increasing oxygen content during milling, whereas the amount of basic
272 functional groups decreased (Figure 6S). The decrease in the amount of basic groups was
273 approximately half the increase in the amount of acidic groups; therefore, the total number
274 of functional groups was increased. When acidic groups were differentiated by selective
275 neutralization with bases of different basicities, the data indicated increases in the amounts
276 of phenolic hydroxyl, lactonic, and carboxylic groups (Figure 4). In addition, the rates of
277 increase against oxygen content were similar for each acidic group regardless initial
278 oxygen content and initial amounts of functional groups. Although W-TKO AC had higher
279 oxygen content, higher amounts of phenolic hydroxyl and lactonic groups, and lower
280 amount of carboxylic groups than W-TK and C-SR ACs, the rates of functional group
281 increases against oxygen contents were similar. Therefore, reaction to introduce these
282 functional groups might occur on the basic structure of AC.

283

284 The basic character of AC with a graphene structure free from oxygen is the result of basic
285 sites arising from delocalized π -electrons as well as the presence of basic groups such as
286 ketones, pyrones, chromenes, ethers, and carbonyls at the particle surface (Shafeeyan et al.
287 2010). Therefore, the decrease in the amount of basic functional groups was likely due to
288 loss of these basic groups and the graphene structure.

289

290 FTIR spectrums of the ACs are shown in Figure 5. As milling progressed, increases were
291 observed for the peaks around 1200 cm^{-1} , which were assigned to C-O and C-OH; the peak
292 around 3400 cm^{-1} , which was assigned to O-H (Barroso-Bogeat et al. 2014, Fanning and
293 Vannice 1993, Shafeeyan et al. 2010); and the peak around 1580 cm^{-1} , which was ascribed
294 to the presence of vicinal hydroxyl groups (Fuente et al. 2003) (Note: while the increase

295 of the peak 3400 cm^{-1} was distinct for W-TK and C-SR ACs, the increase was faint for W-
296 TKO AC. The reason was not clearly understood). Overall, both the Boehm and FTIR data
297 indicate the formation of carboxylic and phenolic hydroxyl groups. The peak around 1700
298 cm^{-1} , which was assigned to C=O in acidic (carboxylic and lactonic) and basic groups
299 (ketone, pyrone, etc.), was unchanged. The increase in the amount of acidic groups and the
300 decrease in the amounts of basic groups may have cancelled out any observable change in
301 the absorbance around 1700 cm^{-1} , particularly if basic groups were converted to acidic
302 groups.

303

304 Thus, the results of the three analyses (elemental, Boehm titration, and FTIR) were in
305 agreement, indicating that the micro-milling produced oxygen/hydrogen-containing acidic
306 functional groups, including phenolic hydroxyl and carboxylic functional groups. The
307 extent of the acidic group increase was twice that of the basic group decrease, and thus the
308 formation of acidic groups could not have been entirely due to the conversion of basic
309 groups to acidic groups. New surfaces generated by the fracture of particles during milling
310 exhibit high chemical reactivity due to unsaturated carbon atoms at the graphene edge,
311 which are crystallographically disordered and can be functionalized by oxygen or
312 hydrogen. Welham and Williams (1998) ball-milled graphite and AC in a vacuum for up
313 to 1000 h and reported that the ignition temperature of graphite decreased with increasing
314 milling time and that this decrease was concomitant with a large increase in non-crystalline
315 carbon. Thus, the formation of oxygen/hydrogen-containing groups is likely related to
316 increased reactivity due to a reduction in crystallinity at the particle surface.

317

318 Finally, the hypothesis that the reduction of adsorption capacity by micro-milling is due to
319 the formation of oxygen-containing functional groups was verified. These functional

320 groups were acidic oxygen/hydrogen-containing functional groups including carboxylic,
321 phenolic hydroxyl and lactone groups. This conclusion is in consistency with the previous
322 researches for chemical and thermal-treated ACs of conventional-size powdered and
323 granular forms which report that MIB adsorptions were impacted by total surface acidity
324 (Chestnutt Jr et al. 2007, Tennant and Mazyck 2007).

325

326 ***3.3 Factors affecting the production of oxygen/hydrogen-containing functional groups***

327

328 **3.3.1. Contribution of DO**

329

330 To investigate the cause of the oxygen/hydrogen content increase, we operated the mill
331 under several operation conditions. Pan et al. (2017a) reported that AC oxidation was
332 partially attenuated when the oxygen in the water and adsorbed on the AC were removed
333 before milling, the introduction of oxygen during milling was prevented, and the rotational
334 speed in the milling was lowered from 12 to 8 m/s.

335

336 In our study, we measured DO concentration during milling (Figure 6). At a milling speed
337 of 8 m/s, DO concentration decreased slowly and was reduced by half at 240 min of milling.
338 However, at the higher milling speed of 12 m/s, we observed a dramatic decrease of DO;
339 by 100 min after the start of milling, DO was <1 mg/L. Although the DO concentration
340 dropped, we found that the oxygen content of the ACs gradually increased with increasing
341 milling time, even after 100 min (Figure 7). No change of DO concentration was observed
342 without AC slurry (data not shown).

343

344 We then converted the oxygen content (mass of oxygen per mass of AC) to mass of oxygen
345 per liter of AC slurry because the grinding was conducted at a fixed AC mass concentration
346 (Figure 7). Before grinding, the oxygen mass per liter of AC slurry was around 300 mg-
347 O/L. However, under high-speed milling (12 m/s) it had increased to around 700 mg-O/L
348 at 120 min, and under low-speed milling (8 m/s) it had increased to around 500 mg-O/L at
349 180 min. These changes in mass of oxygen per liter of AC slurry (200 and 400 mg-O/L for
350 low- and high-speed milling, respectively) were very large compared with the change of
351 DO. Any reaction that increases the oxygen content of AC and promotes the formation of
352 oxygen-containing functional groups could have accompanied the consumption of DO in
353 the slurry, but the extent of the DO decrease in the slurry did not quantitatively explain the
354 increase in oxygen content. However, the possibility remained that DO introduced from
355 the air to the slurry may have caused the increase of oxygen content in the ACs.

356

357 To confirm the contribution of DO to the oxygen content increase, we milled AC particles
358 under anoxic conditions and then determined the elemental composition of the AC particles.
359 Figure 7 (closed plots) shows the change of oxygen content of the ACs during anoxic
360 milling. The change of oxygen content with time during anoxic milling was smaller than
361 that observed during normal milling. Thus, the DO in AC slurry does affect the oxygen
362 increase in AC particles, but the effect is limited. The increase of oxygen content in the
363 AC particles was influenced by milling speed, even under anoxic conditions, again
364 indicating that the DO was not strongly related to the oxygen content increase in AC
365 particles. These results verified that DO was not a major cause of the oxygen content
366 increase.

367

368 3.3.2 Oxidant formation during milling

369

370 Water containing reducing substances (SO_3^- and NO_2^- ions) were introduced into the
371 milling chamber, and then the mill was operated (details are described in SI). There were
372 no or insignificant change in the concentrations (Figures 7S and 8S). In reference to the
373 generation of gaseous hydrogen during the mechanochemical treatment of metal oxides in
374 water (Domen et al. 2000, Hara et al. 2000, Kazunari et al. 2000), we tried to collect gas
375 present above the water; however, no gas was collected, and so we concluded that no gas
376 was generated.

377

378 Next, the possibility of the formation of an oxidant, hydroxyl radical, during milling was
379 investigated by using two probe compounds: 1,4-dioxane and salicylic acid (details are
380 described in SI). 1,4-Dioxane is decomposed by hydroxyl radical but not by oxygen, ozone,
381 or chlorine (Adams et al. 1994, Coleman et al. 2007, Hill et al. 1997, Klečka and Gonsior
382 1986, Matsushita et al. 2015, Suh and Mohseni 2004). During milling, however, 1,4-
383 dioxane concentration did not change (Figure 9S). Salicylic acid is also decomposed by
384 hydroxyl radical (Jen et al. 1998, Karnik et al. 2007, Quan et al. 2007, Tabatabaei and
385 Abbott 1999) to 2,3-dihydroxybenzoic acid (2,3-DHBA) and 2,5-dihydroxybenzoic acid
386 (2,5-DHBA) (Figure 10S). During operation of the micro-mill, we observed a decrease of
387 salicylic acid concentration (Figure 11S), but the formation of 2,3-DHBA and 2,5-DHBA
388 was not observed (Figure 12S). Thus, we concluded that hydroxyl radicals were not formed
389 during milling. The decrease in salicylic acid would be caused by any mechanochemical
390 reaction, but no specific mechanism was identified.

391

392 3.3.3 Role of water in the formation of oxygen/hydrogen-containing functional groups

393

394 The results of the investigations described in the previous two sections suggested that a
395 mechanochemical reaction that produced oxygen/hydrogen-containing functional groups
396 in the ACs occurred during milling. Newly formed surfaces of milled AC exhibit extremely
397 high chemical reactivity because of a lack of chemical bond saturation, resulting in surface
398 re-formation by chemical reaction with the surrounding water (Balaz et al. 2013, Berndt
399 2004).

400

401 Oxygen and hydrogen in the oxygen/hydrogen-containing functional groups formed on the
402 AC particle surface during milling could have come from water molecules including
403 hydroxide ions. To explore this possibility, we milled a SPAC_L (W-TK) slurry containing
404 water-¹⁸O. Figure 8 shows the change of $\delta^{18}\text{O}$ as the particle size decreased during anoxic
405 milling. We observed a marked increase in the amount of $\delta^{18}\text{O}$ in SSPAC after milling in
406 water-¹⁸O compared with the amount in SPAC_L. In addition, the amount of $\delta^{18}\text{O}$ in SSPAC
407 was higher when a longer milling time was used (6 h vs. 2 h). In contrast, $\delta^{18}\text{O}$ did not
408 increase when the SSPAC was simply mixed with water-¹⁸O for 2–6 h. These results
409 clearly indicate that oxygen from the surrounding water was introduced into the AC when
410 the AC particles were milled.

411

412 The diamonds in Figure 8 are $\delta^{18}\text{O}$ values that were predicted by taking the mass balance
413 of the oxygen content under the assumption that the additional oxygen atoms in the SSPAC
414 after micro-milling originated entirely from the surrounding water and were characterized
415 by an ¹⁸O/¹⁶O ratio identical to that of the surrounding water. The observed $\delta^{18}\text{O}$ values
416 were lower than the predicted values. We assume this discrepancy was due to exchange
417 of ¹⁸O with ¹⁶O during sample capsulation, transportation, and storage before isotope

418 analysis. This was inferred from the following two results. First, the $\delta^{18}\text{O}$ values were
419 higher when the AC samples were capsuled under anoxic conditions in a glovebox filled
420 with nitrogen gas. Second, the $\delta^{18}\text{O}$ values were lower with longer elapsed time between
421 sample production and analysis (Figure 15S). The isotope analysis shown in Figure 8 was
422 conducted 5 days after the SSPAC samples were produced; 5 days was the minimum
423 interval for sample transportation. There is also the possibility of a kinetic isotope effect
424 in which water- ^{18}O exhibited lower rate of reaction than water- ^{16}O , so the $^{18}\text{O}/^{16}\text{O}$ ratio of
425 the oxygen-containing groups formed by the reaction would be lower than that of the water
426 (Fry 2007).

427

428 Overall, the data indicate that oxygen/hydrogen-containing functional groups in the AC
429 came from the water used to make the AC slurry. Specifically, hydroxide ions formed by
430 the dissociation of water likely reacted with the newly formed surfaces of milled AC to
431 form oxygen/hydrogen-containing functional groups. This conclusion is further supported
432 by the decrease of the pH of the AC slurry with increasing oxygen content during milling
433 (Figure 16S).

434

435

436 **4. Conclusions**

437

438 1) Adsorption capacities of MIB, geosmin, and bentazone increased with decreasing
439 particle diameter in the micron size range, but decreased with decreasing particle diameter
440 in the submicron size range. The reduction of adsorption capacity by micro-milling was
441 due to a decrease of hydrophobicity at the AC particle surface due to the formation of
442 acidic functional groups containing oxygen and hydrogen.

443

444 2) With increasing duration of micro-milling, the amount of acidic functional groups, as
445 determined by Boehm method, as well as the oxygen and hydrogen content, as determined
446 by elemental analysis, in the AC particles was increased. The acidic functional groups
447 included carboxylic, phenolic hydroxyl and lactone groups. With increased duration of
448 micro-milling, the total (acidic and basic) number of functional groups increased, whereas
449 the amount of basic functional groups decreased. With increased duration of milling,
450 increases in FTIR peaks at 1200, 1580, and 3400 cm^{-1} were observed. These peaks were
451 assigned to carboxylic and phenolic hydroxyl functional groups.

452

453 3) The increase of oxygen content in AC particles during milling was somewhat attenuated
454 under anoxic conditions. The DO concentration in the slurry decreased during milling at
455 high-speed but not at low-speed. However, the decrease of oxygen content was much
456 smaller than the increase of oxygen content in AC particles. Therefore, oxidation of the
457 AC particles by DO played a minor role in the increase of oxygen content. No gas
458 production was observed, nor was there any evidence of oxidant formation.

459

460 4) When AC was milled in water- ^{18}O , the ^{18}O content of the AC increased. The pH of AC
461 slurry decreased during micro-milling. Therefore, the oxygen in the oxygen/hydrogen-
462 containing functional groups originated from the surrounding water, probably hydroxide
463 ion. The new oxygen/hydrogen-containing functional groups in the AC likely arose from
464 a mechanochemical reaction that occurred during the milling process. Newly formed
465 surfaces of milled AC exhibit extremely high chemical reactivity because of the chemical
466 bond unsaturation and therefore underwent surface re-formation by chemical reaction with

467 hydroxide ion in the surrounding water and the formation of oxygen/hydrogen-containing
468 functional groups.

469

470

471

472 **Acknowledgments**

473

474 This work was supported by JSPS (Japan Society for the Promotion of Science) KAKENHI
475 Grant Number JP16H06362. The authors gratefully acknowledge Futamura Chemical and
476 Osaka Gas Chemicals for providing PAC samples.

477

478

479

480

481

482 **References**

- 483 Adams, C.D., Scanlan, P.A. and Secrist, N.D. (1994) Oxidation and Biodegradability Enhancement
484 of 1,4-Dioxane Using Hydrogen Peroxide and Ozone. *Environmental Science & Technology*
485 28(11), 1812-1818.
- 486 Amaral, P., Partlan, E., Li, M., Lapolli, F., Mefford, O.T., Karanfil, T. and Ladner, D.A. (2016)
487 Superfine powdered activated carbon (S-PAC) coatings on microfiltration membranes: Effects of
488 milling time on contaminant removal and flux. *Water Research* 100, 429-438.
- 489 Ando, N., Matsui, Y., Kurotobi, R., Nakano, Y., Matsushita, T. and Ohno, K. (2010) Comparison of
490 natural organic matter adsorption capacities of super-powdered activated carbon and
491 powdered activated Carbon. *Water Research* 44(14), 4127-4136.
- 492 Balaz, P., Achimovicova, M., Balaz, M., Billik, P., Cherkezova-Zheleva, Z., Criado, J.M., Delogu, F.,
493 Dutkova, E., Gaffet, E., Gotor, F.J., Kumar, R., Mitov, I., Rojac, T., Senna, M., Streletskii, A. and
494 Wieczorek-Ciurowa, K. (2013) Hallmarks of mechanochemistry: from nanoparticles to
495 technology. *Chemical Society Reviews* 42(18), 7571-7637.
- 496 Barroso-Bogeat, A., Alexandre-Franco, M., Fernández-González, C. and Gómez-Serrano, V.
497 (2014) FT-IR Analysis of Pyrone and Chromene Structures in Activated Carbon. *Energy & Fuels*
498 28(6), 4096-4103.

499 Berndt, C.C. (2004) Handbook of Thermal Spray Technology. Davis, J.R. (ed), pp. 147-158, ASM
500 International.

501 Biniak, S., Szymański, G., Siedlewski, J. and Świątkowski, A. (1997) The characterization of
502 activated carbons with oxygen and nitrogen surface groups. Carbon 35(12), 1799-1810.

503 Boehm, H.P. (1966) Advances in Catalysis, vol. 16. Eley, D.D., Pines, H. and Weisz, P.B. (eds), p.
504 179, Academic Press, New York.

505 Boehm, H.P. (2002) Surface oxides on carbon and their analysis: a critical assessment. Carbon
506 40(2), 145-149.

507 Bonvin, F., Jost, L., Randin, L., Bonvin, E. and Kohn, T. (2016) Super-fine powdered activated
508 carbon (SPAC) for efficient removal of micropollutants from wastewater treatment plant
509 effluent. Water Research 90, 90-99.

510 Chestnutt Jr, T.E., Bach, M.T. and Mazyck, D.W. (2007) Improvement of thermal reactivation of
511 activated carbon for the removal of 2-methylisoborneol. Water Research 41(1), 79-86.

512 Coleman, H.M., Vimonses, V., Leslie, G. and Amal, R. (2007) Degradation of 1,4-dioxane in water
513 using TiO₂ based photocatalytic and H₂O₂/UV processes. Journal of Hazardous Materials
514 146(3), 496-501.

515 Considine, R., Denoyel, R., Pendleton, P., Schumann, R. and Wong, S.-H. (2001) The influence of
516 surface chemistry on activated carbon adsorption of 2-methylisoborneol from aqueous solution.
517 Colloids and Surfaces A: Physicochemical and Engineering Aspects 179(2-3), 271-280.

518 Domen, K., Ikeda, S., Takata, T., Tanaka, A., Hara, M. and Kondo, J.N. (2000) Mechano-catalytic
519 overall water-splitting into hydrogen and oxygen on some metal oxides. Applied Energy 67(1),
520 159-179.

521 Dunn, S.E. and Knappe, D.R.U. (2013) DBP precursor and micropollutant removal by powdered
522 activated carbon, Water Research Foundation, Denver, CO, USA.

523 Ellerie, J.R., Apul, O.G., Karanfil, T. and Ladner, D.A. (2013) Comparing graphene, carbon
524 nanotubes, and superfine powdered activated carbon as adsorptive coating materials for
525 microfiltration membranes. Journal of Hazardous Materials 261(0), 91-98.

526 Fanning, P.E. and Vannice, M.A. (1993) A DRIFTS study of the formation of surface groups on
527 carbon by oxidation. Carbon 31(5), 721-730.

528 Fry, B. (2007) Stable Isotope Ecology, Springer New York.

529 Fuente, E., Menéndez, J.A., Díez, M.A., Suárez, D. and Montes-Morán, M.A. (2003) Infrared
530 Spectroscopy of Carbon Materials: A Quantum Chemical Study of Model Compounds. The
531 Journal of Physical Chemistry B 107(26), 6350-6359.

532 Hara, M., Komoda, M., Hasei, H., Yashima, M., Ikeda, S., Takata, T., Kondo, J.N. and Domen, K.
533 (2000) A Study of Mechano-Catalysts for Overall Water Splitting. The Journal of Physical
534 Chemistry B 104(4), 780-785.

535 Heijman, S.G.J., Hamad, J.Z., Kennedy, M.D., Schippers, J. and Amy, G. (2009) Submicron
536 powdered activated carbon used as a pre-coat in ceramic micro-filtration. Desalination and
537 Water Treatment 9(1-3), 86-91.

538 Hill, R.R., Jeffs, G.E. and Roberts, D.R. (1997) Photocatalytic degradation of 1,4-dioxane in
539 aqueous solution. Journal of Photochemistry and Photobiology A: Chemistry 108(1), 55-58.

540 Jen, J.-F., Leu, M.-F. and Yang, T.C. (1998) Determination of hydroxyl radicals in an advanced
541 oxidation process with salicylic acid trapping and liquid chromatography. Journal of
542 Chromatography A 796(2), 283-288.

543 Jiang, W., Xiao, F., Wang, D.S., Wang, Z.C. and Cai, Y.H. (2015) Removal of emerging
544 contaminants by pre-mixed PACl and carbonaceous materials. RSC Advances 5(45), 35461-
545 35468.

546 Kanaya, S., Kawase, Y. and Mima, S. (2015) Drinking water treatment using superfine PAC
547 (SPAC): design and successful operation history in full-scale plant, pp. 624-631, American Water
548 Works Association, Salt Lake City, Utah, USA

549 Karnik, B.S., Davies, S.H., Baumann, M.J. and Masten, S.J. (2007) Use of Salicylic Acid as a Model
550 Compound to Investigate Hydroxyl Radical Reaction in an Ozonation–Membrane Filtration
551 Hybrid Process. *Environmental Engineering Science* 24(6), 852-860.

552 Kazunari, D., N., K.J., Michikazu, H. and Tsuyoshi, T. (2000) Photo- and Mechano-Catalytic
553 Overall Water Splitting Reactions to Form Hydrogen and Oxygen on Heterogeneous Catalysts.
554 *Bulletin of the Chemical Society of Japan* 73(6), 1307-1331.

555 Klečka, G.M. and Gonsior, S.J. (1986) Removal of 1,4-dioxane from wastewater. *Journal of*
556 *Hazardous Materials* 13(2), 161-168.

557 Matsui, Y., Fukuda, Y., Murase, R., Aoki, N., Mima, S., Inoue, T. and Matsushita, T. (2004) Micro-
558 ground powdered activated carbon for effective removal of natural organic matter during water
559 treatment. *Water Science & Technology: Water Supply* 4(4), 155-163.

560 Matsui, Y., Nakao, S., Sakamoto, A., Taniguchi, T., Pan, L., Matsushita, T. and Shirasaki, N. (2015)
561 Adsorption capacities of activated carbons for geosmin and 2-methylisoborneol vary with
562 activated carbon particle size: Effects of adsorbent and adsorbate characteristics. *Water*
563 *Research* 85, 95-102.

564 Matsui, Y., Nakao, S., Taniguchi, T. and Matsushita, T. (2013) Geosmin and 2-methylisoborneol
565 removal using superfine powdered activated carbon: Shell adsorption and branched-pore
566 kinetic model analysis and optimal particle size. *Water Research* 47(8), 2873-2880.

567 Matsui, Y., Yoshida, T., Nakao, S., Knappe, D.R.U. and Matsushita, T. (2012) Characteristics of
568 competitive adsorption between 2-methylisoborneol and natural organic matter on superfine
569 and conventionally sized powdered activated carbons. *Water Research* 46(15), 4741-4749.

570 Matsushita, T., Hirai, S., Ishikawa, T., Matsui, Y. and Shirasaki, N. (2015) Decomposition of 1,4-
571 dioxane by vacuum ultraviolet irradiation: Study of economic feasibility and by-product
572 formation. *Process Safety and Environmental Protection* 94, 528-541.

573 Noh, J.S. and Schwarz, J.A. (1990) Effect of HNO₃ treatment on the surface acidity of activated
574 carbons. *Carbon* 28(5), 675-682.

575 Pan, L., Matsui, Y., Matsushita, T. and Shirasaki, N. (2016) Superiority of wet-milled over dry-
576 milled superfine powdered activated carbon for adsorptive 2-methylisoborneol removal. *Water*
577 *Research* 102, 516-523.

578 Pan, L., Nishimura, Y., Takaesu, H., Matsui, Y., Matsushita, T. and Shirasaki, N. (2017a) Effects of
579 decreasing activated carbon particle diameter from 30 μm to 140 nm on equilibrium adsorption
580 capacity. *Water Research* 124, 425-434.

581 Pan, L., Takagi, Y., Matsui, Y., Matsushita, T. and Shirasaki, N. (2017b) Micro-milling of spent
582 granular activated carbon for its possible reuse as an adsorbent: Remaining capacity and
583 characteristics. *Water Research* 114, 50-58.

584 Partlan, E., Davis, K., Ren, Y., Apul, O.G., Mefford, O.T., Karanfil, T. and Ladner, D.A. (2016) Effect
585 of bead milling on chemical and physical characteristics of activated carbons pulverized to
586 superfine sizes. *Water Research* 89, 161-170.

587 Pendleton, P., Wong, S.H., Schumann, R., Levay, G., Denoyel, R. and Rouquero, J. (1997)
588 Properties of activated carbon controlling 2-Methylisoborneol adsorption. *Carbon* 35(8), 1141-
589 1149.

590 Pendleton, P., Wu, S.H. and Badalyan, A. (2002) Activated carbon oxygen content influence on
591 water and surfactant adsorption. *J Colloid Interface Sci* 246(2), 235-240.

592 Quan, X., Zhang, Y., Chen, S., Zhao, Y. and Yang, F. (2007) Generation of hydroxyl radical in
593 aqueous solution by microwave energy using activated carbon as catalyst and its potential in
594 removal of persistent organic substances. *Journal of Molecular Catalysis A: Chemical* 263(1),
595 216-222.

596 Quinlivan, P.A., Li, L. and Knappe, D.R. (2005) Effects of activated carbon characteristics on the
597 simultaneous adsorption of aqueous organic micropollutants and natural organic matter. *Water*
598 *Research* 39(8), 1663-1673.

599 Shafeeyan, M.S., Daud, W.M.A.W., Houshmand, A. and Shamiri, A. (2010) A review on surface
600 modification of activated carbon for carbon dioxide adsorption. *Journal of Analytical and*
601 *Applied Pyrolysis* 89(2), 143-151.
602 Suh, J.H. and Mohseni, M. (2004) A study on the relationship between biodegradability
603 enhancement and oxidation of 1,4-dioxane using ozone and hydrogen peroxide. *Water*
604 *Research* 38(10), 2596-2604.
605 Tabatabaei, A.R. and Abbott, F.S. (1999) LC/MS analysis of hydroxylation products of salicylate
606 as an indicator of in vivo oxidative stress. *Free Radical Biology and Medicine* 26(7), 1054-1058.
607 Tennant, M.F. and Mazyck, D.W. (2007) The role of surface acidity and pore size distribution in
608 the adsorption of 2-methylisoborneol via powdered activated carbon. *Carbon* 45(4), 858-864.
609 Welham, N.J. and Williams, J.S. (1998) Extended milling of graphite and activated carbon.
610 *Carbon* 36(9), 1309-1315.
611 WHO (2011) Guidelines for drinking-water quality, World Health Organization, Geneva,
612 Switzerland.

613

List of Figures

Figure 1. Change of adsorption capacity with AC particle size. The values on the y-axis were quantified in terms of the solid-phase concentration for an equilibrium liquid-phase concentration of 50 ng/L for MIB and geosmin and 5 µg/L for bentazone (see also Figure 1S-4S).

Figure 2. Correlation between adsorption capacity and oxygen content. The values on the y-axis were quantified in terms of the solid-phase concentration for an equilibrium liquid-phase concentration of 50 ng/L for MIB and geosmin and 5 µg/L for bentazone (see also Figure 1S-4S).

Figure 3. Changes of O, H, C, N, and S content versus AC particle diameter during milling. The lower right panel is a plot of the relationship between the O and H content.

Figure 4. Change in the amount of phenolic hydroxyl, lactone, carboxyl, and basic functional groups versus oxygen content during milling. Upper panels are for W-TK AC; middle panels are for C-SR; lower panels are for W-TKO.

Figure 5. FTIR spectra of the ACs. Upper panels are for the 1st and 2nd milling runs of C-SR AC; lower left panel is for W-TK; lower right panel is for W-TKO.

Figure 6. Change of DO concentration during milling of W-TK AC.

Figure 7. Change of oxygen content of AC during milling. W-TK AC (10 g/L) was used; therefore, 10% oxygen content was converted to 1000 mg oxygen per liter of slurry.

Figure 8. Isotope ratio for oxygen-18 (^{18}O) and oxygen-16 (^{16}O). Predicted values (closed diamond plots) were obtained by taking the mass balance of the oxygen content under the assumption that the additional oxygen atoms in the SSPAC after milling originated entirely from the surrounding water and were characterized by an $^{18}\text{O}/^{16}\text{O}$ ratio identical to that of the surrounding water. Control values (closed rectangular plots) were obtained by stirring SSPAC water- ^{18}O . The carbon was W-TK.

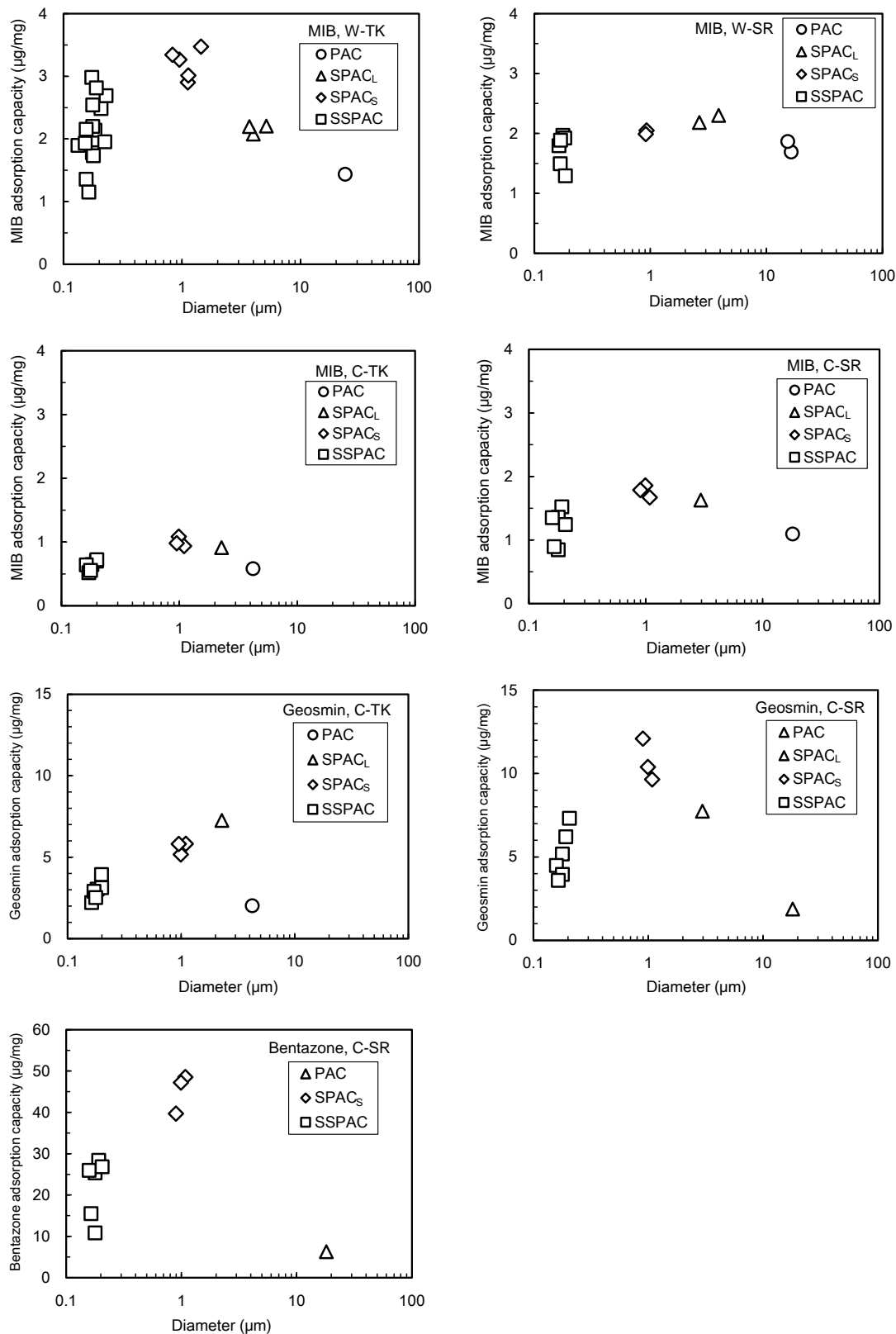


Figure 1. Change of adsorption capacity with AC particle size. The values on the y-axis were quantified in terms of the solid-phase concentration for an equilibrium liquid-phase concentration of 50 ng/L for MIB and geosmin and 5 μg/L for bentazone (see also Figure 1S-4S).

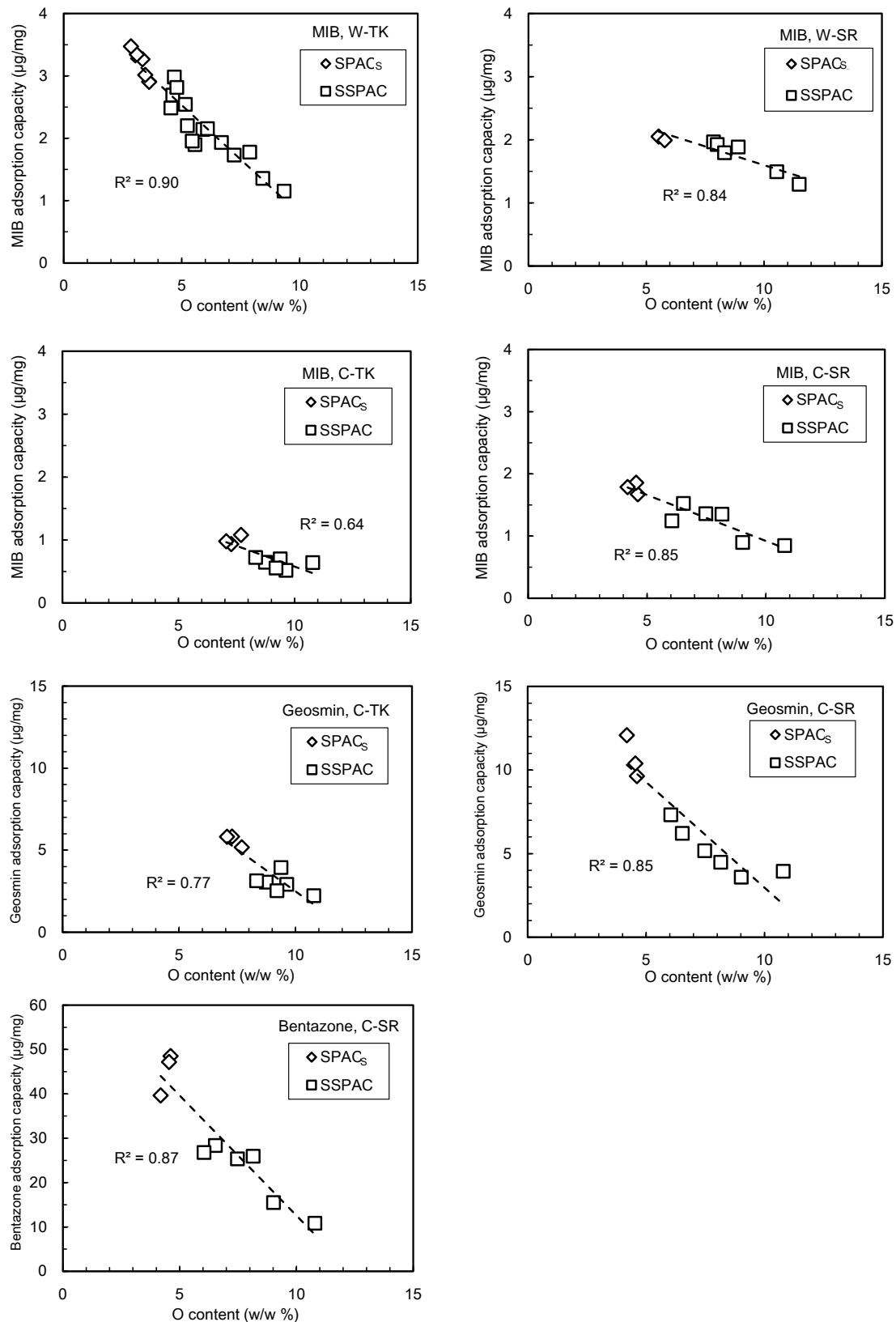


Figure 2. Correlation between adsorption capacity and oxygen content. The values on the y-axis were quantified in terms of the solid-phase concentration for an equilibrium liquid-phase concentration of 50 ng/L for MIB and geosmin and 5 µg/L for bentazone (see also Figure 1S-4S).

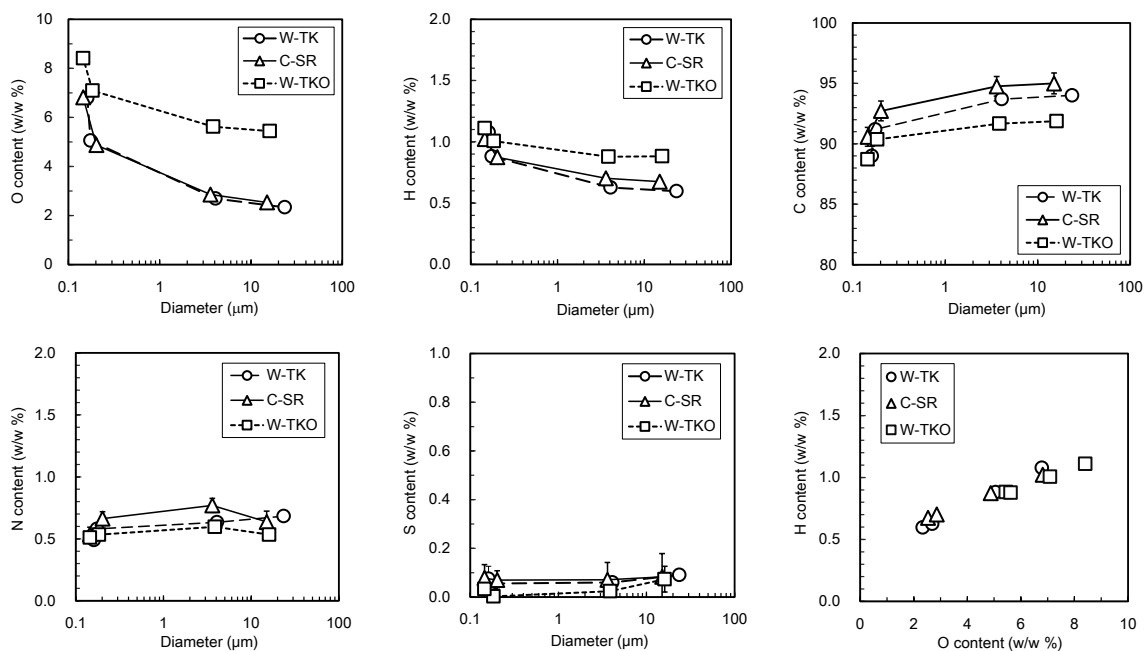


Figure 3. Changes of O, H, C, N, and S content versus AC particle diameter during milling. The lower right panel is a plot of the relationship between the O and H content.

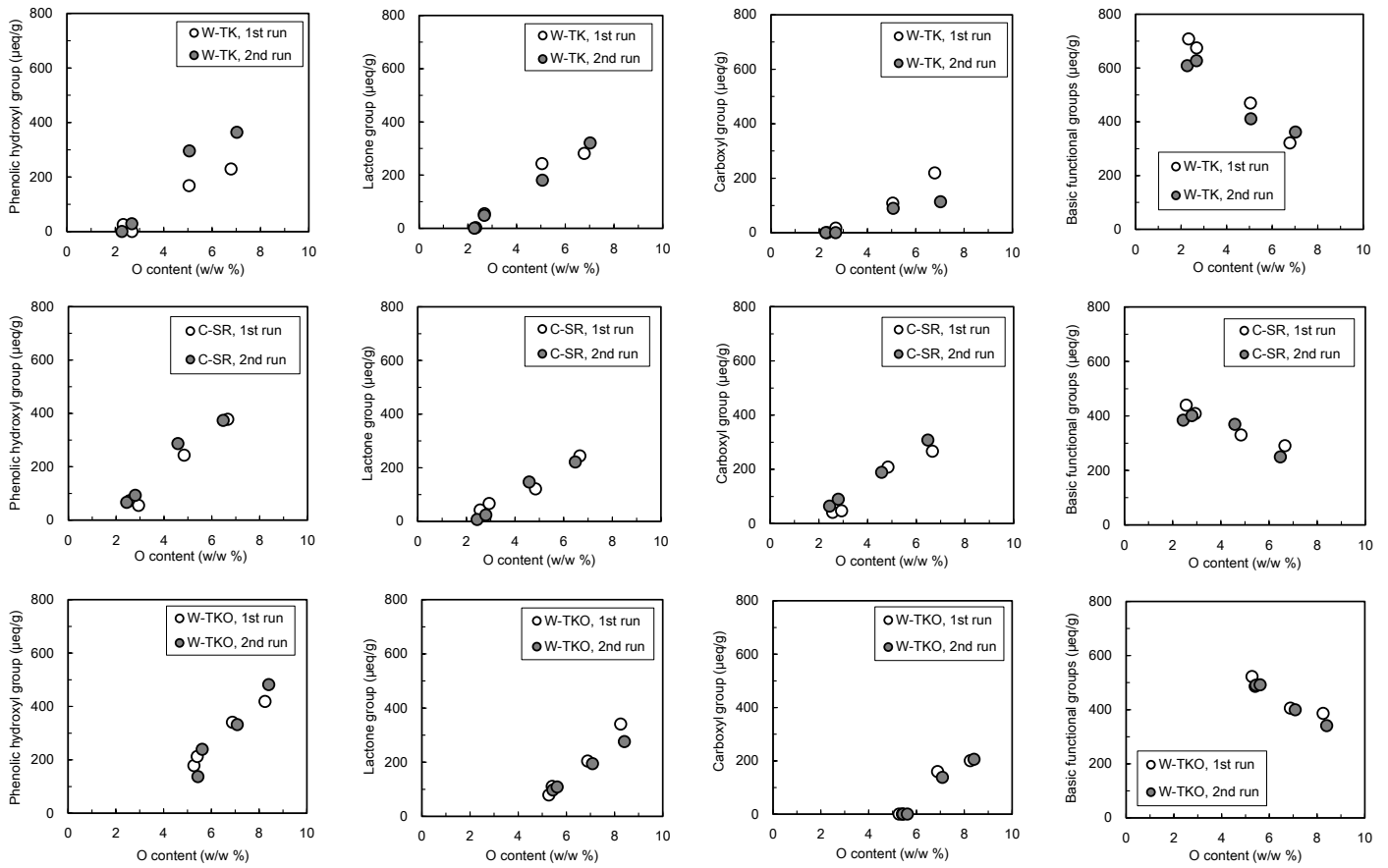


Figure 4. Change in the amount of phenolic hydroxyl, lactone, carboxyl, and basic functional groups versus oxygen content during milling. Upper panels are for W-TK AC; middle panels are for C-SR; lower panels are for W-TKO.

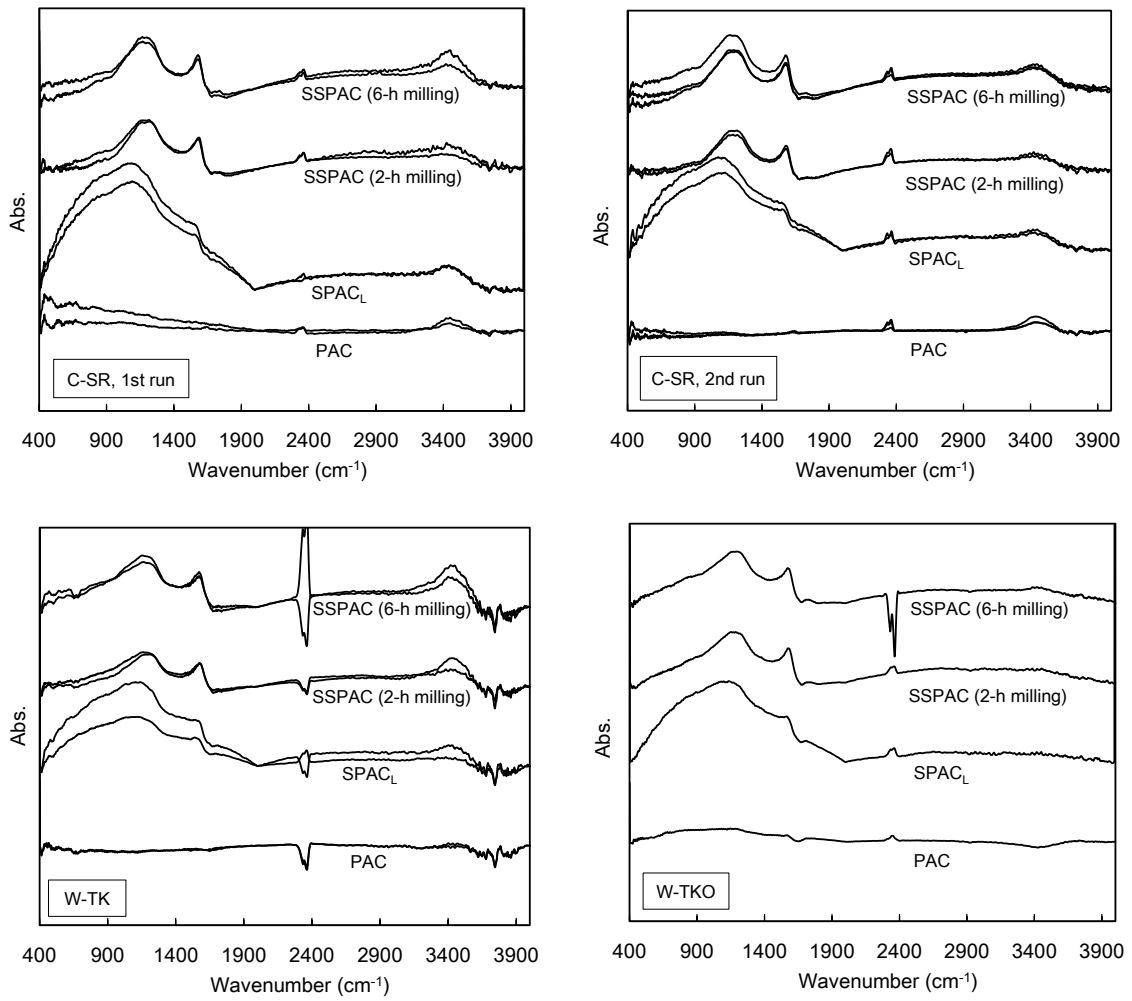


Figure 5. FTIR spectra of the ACs. Upper panels are for the 1st and 2nd milling runs of C-SR AC; lower left panel is for W-TK; lower right panel is for W-TKO.

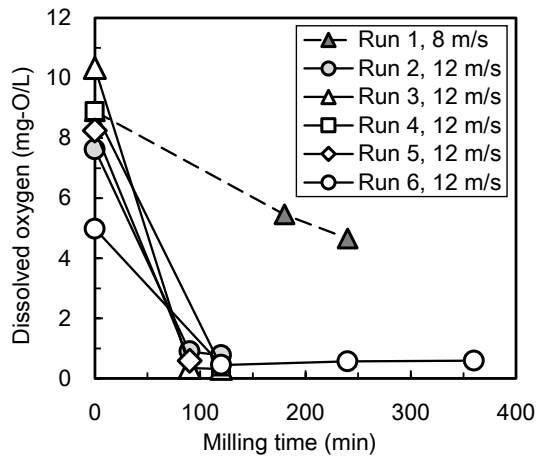


Figure 6. Change of DO concentration during milling of W-TK AC.

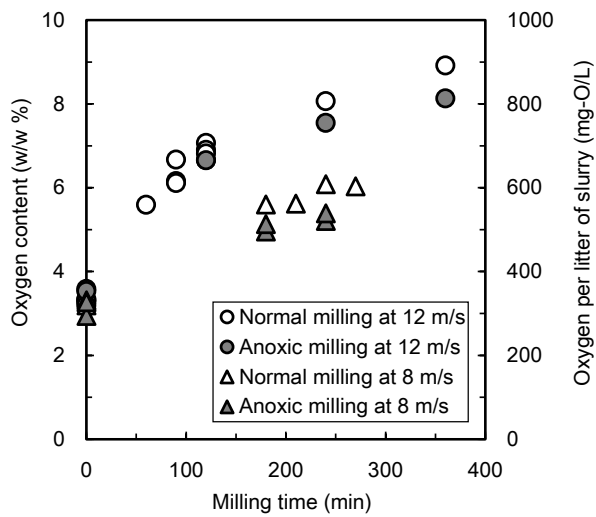


Figure 7. Change of oxygen content of AC during milling. W-TK AC (10 g/L) was used; therefore, 10% oxygen content was converted to 1000 mg oxygen per liter of slurry.

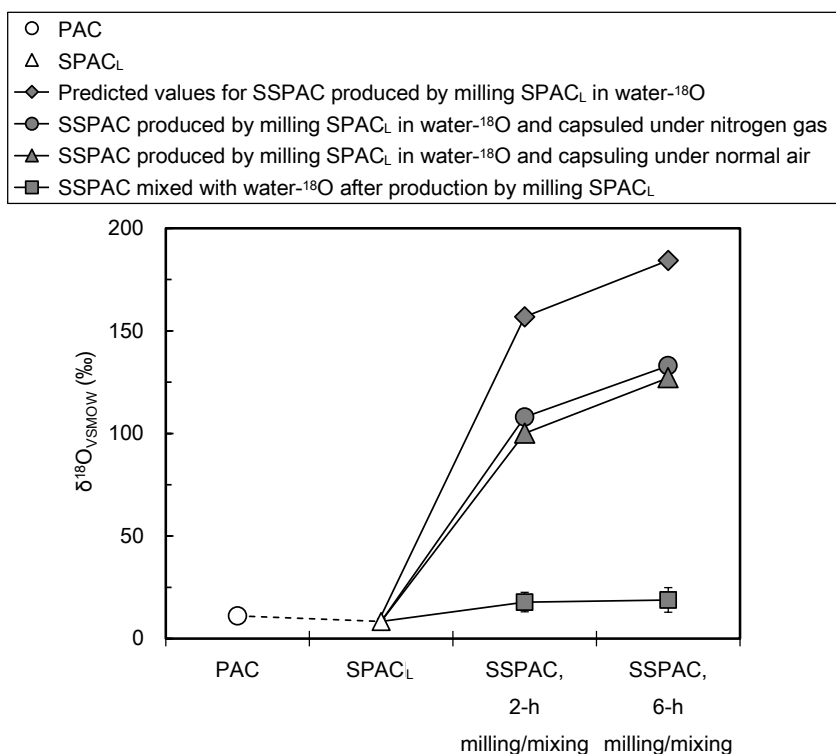


Figure 8. Isotope ratio for oxygen-18 (¹⁸O) and oxygen-16 (¹⁶O). Predicted values (closed diamond plots) were obtained by taking the mass balance of the oxygen content under the assumption that the additional oxygen atoms in the SSPAC after milling originated entirely from the surrounding water and were characterized by an ¹⁸O/¹⁶O ratio identical to that of the surrounding water. Control values (closed rectangular plots) were obtained by stirring SSPAC water-¹⁸O. The carbon was W-TK.

Supplementary Information

Micro-milling Super-fine Powdered Activated Carbon Decreases Adsorption Capacity by Introducing Oxygen/hydrogen-Containing Functional Groups on Carbon Surface from Water

Hideki Takaesu ^a, Yoshihiko Matsui ^{b,*}, Yuki Nishimura ^a, Taku Matsushita ^b, and Nobutaka Shirasaki ^b

^a Graduate School of Engineering, Hokkaido University, N13W8, Sapporo 060-8628, Japan

^b Faculty of Engineering, Hokkaido University, N13W8, Sapporo 060-8628, Japan

* Corresponding author. Tel./fax: +81-11-706-7280

E-mail address: matsui@eng.hokudai.ac.jp

Investigation of oxidant formation during milling

To investigate the possibility that milling promoted oxidant formation, we determined the concentrations of reducing substances in the milling chamber during milling. Water containing SO_3^- or NO_2^- ions was introduced into the milling chamber, and then the mill was operated (note that the milling chamber did not contain AC particles because the concentrations of the ions would have changed due to ion exchange with the AC surface). At a milling speed of 8 m/s, the concentrations of SO_3^- and NO_2^- ions did not change (Figures 7S and 8S). At the higher milling speed of 12 m/s, SO_3^- concentration decreased slightly and SO_4^- concentration increased slightly, but the extent of the changes was not large when compared with the oxygen content increase (Figures 7S and 7). These results suggest that while oxidation may have occurred in the milling chamber, it did not play a large role in the oxygen content increase. In reference to the generation of gaseous hydrogen during the mechanochemical treatment of metal oxides in water (Domen et al. 2000, Hara et al. 2000, Kazunari et al. 2000), we tried to collect gas present above the water; however, no gas was collected, and so we concluded that no gas was generated.

Next, the possibility of the formation of an oxidant, hydroxyl radical, during milling was investigated. The refractory compound 1,4-dioxane is decomposed by hydroxyl radical but not by oxygen, ozone, or chlorine (Adams et al. 1994, Coleman et al. 2007, Hill et al. 1997, Klečka and Gonsior 1986, Matsushita et al. 2015, Suh and Mohseni 2004). Therefore, we introduced water containing 1,4-dioxane into the milling chamber but observed no change of 1,4-dioxane concentration, even when high-speed milling was used (Figure 9S).

A similar test was conducted for salicylic acid, which is decomposed by hydroxyl radical (Jen et al. 1998, Karnik et al. 2007, Quan et al. 2007, Tabatabaei and Abbott 1999) to 2,3-dihydroxybenzoic acid (2,3-DHBA) and 2,5-dihydroxybenzoic acid (2,5-DHBA). We confirmed the formation of 2,5-DHBA when salicylic acid solution was irradiated by vacuum-ultraviolet light of 185 nm, which produces the hydroxyl radical (Oppenländer 2007) (Figure 10S). During operation of the micro-mill, we observed a decrease of salicylic acid concentration (Figure 11S), but the formation of 2,3-DHBA and 2,5-DHBA was not observed (Figure 12S). Moreover, the decomposition of salicylic acid during micro-milling was not affected by the presence of the radical scavenger tertiary butanol (Figure 13S). Thus, we concluded that hydroxyl radicals were not formed during milling. During the salicylic acid decomposition experiment, the dissolved organic carbon concentration remained unchanged (Figure 14S), whereas the salicylic acid concentration decreased. Therefore, salicylic acid was degraded to organic compounds but not to 2,3-DHBA or 2,5-DHBA, probably by mechanochemical reaction. No specific oxidant that might cause oxidation of the ACs and produce oxygen/hydrogen-containing functional groups was identified.

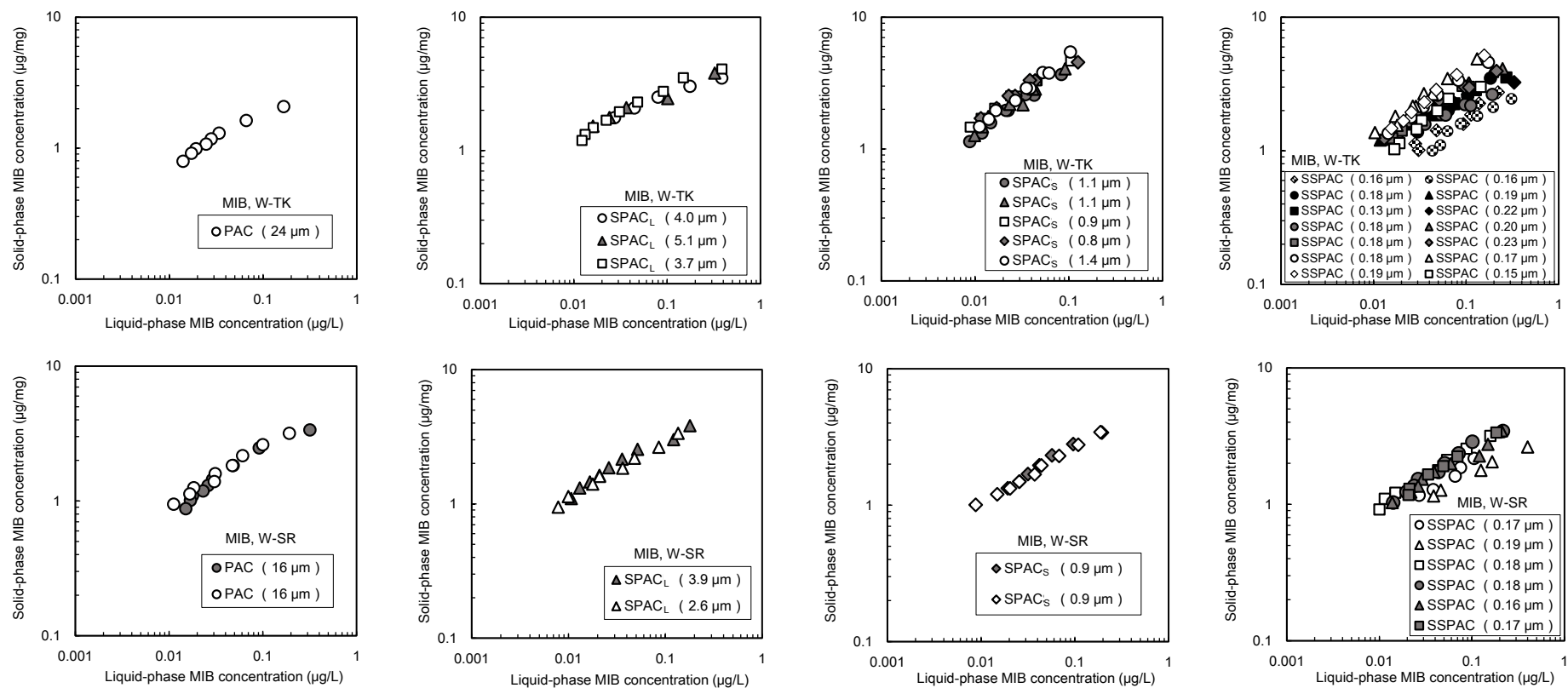


Fig 1S. MIB (2-methylisoborneol) isotherms for W-TK and W-SR ACs (activated carbons) of different particle sizes.

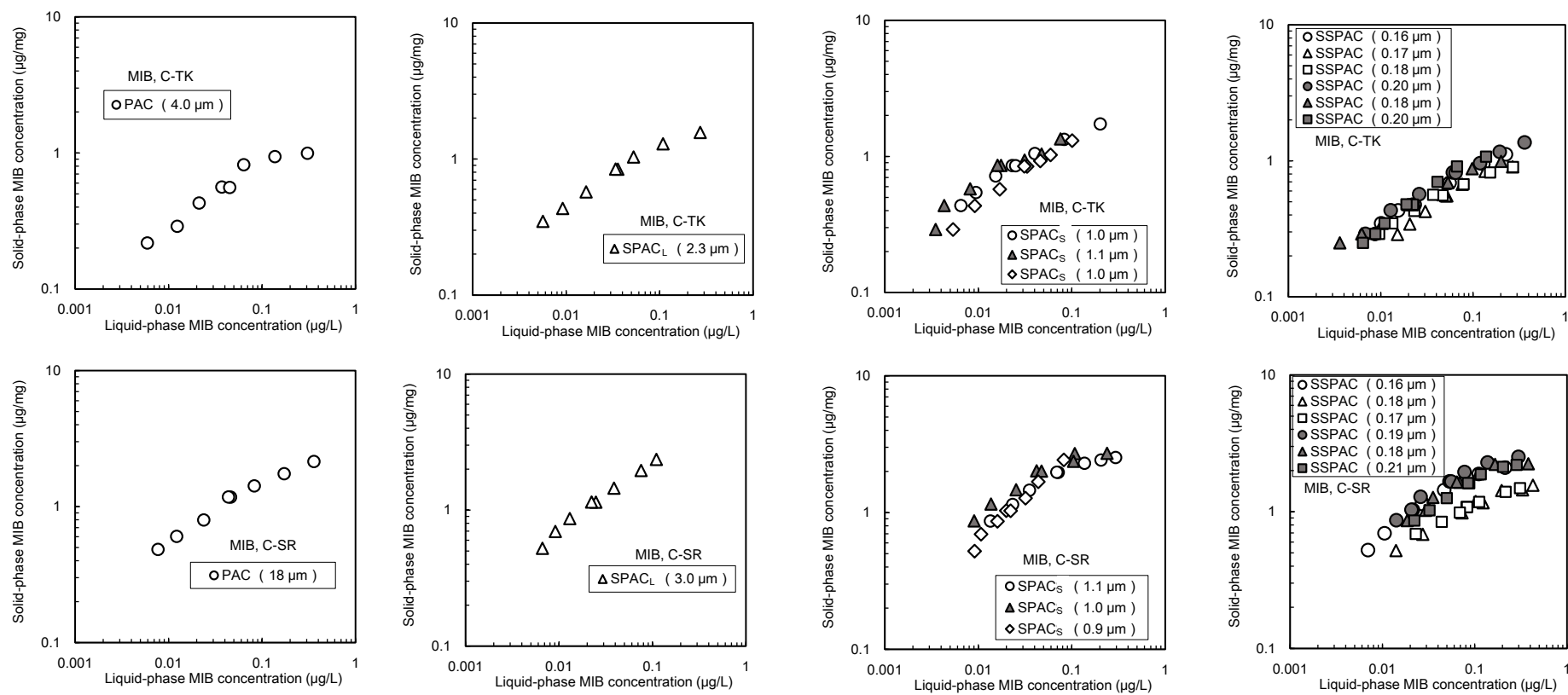


Fig 2S. MIB isotherms for C-TK and C-SR ACs of different particle sizes.

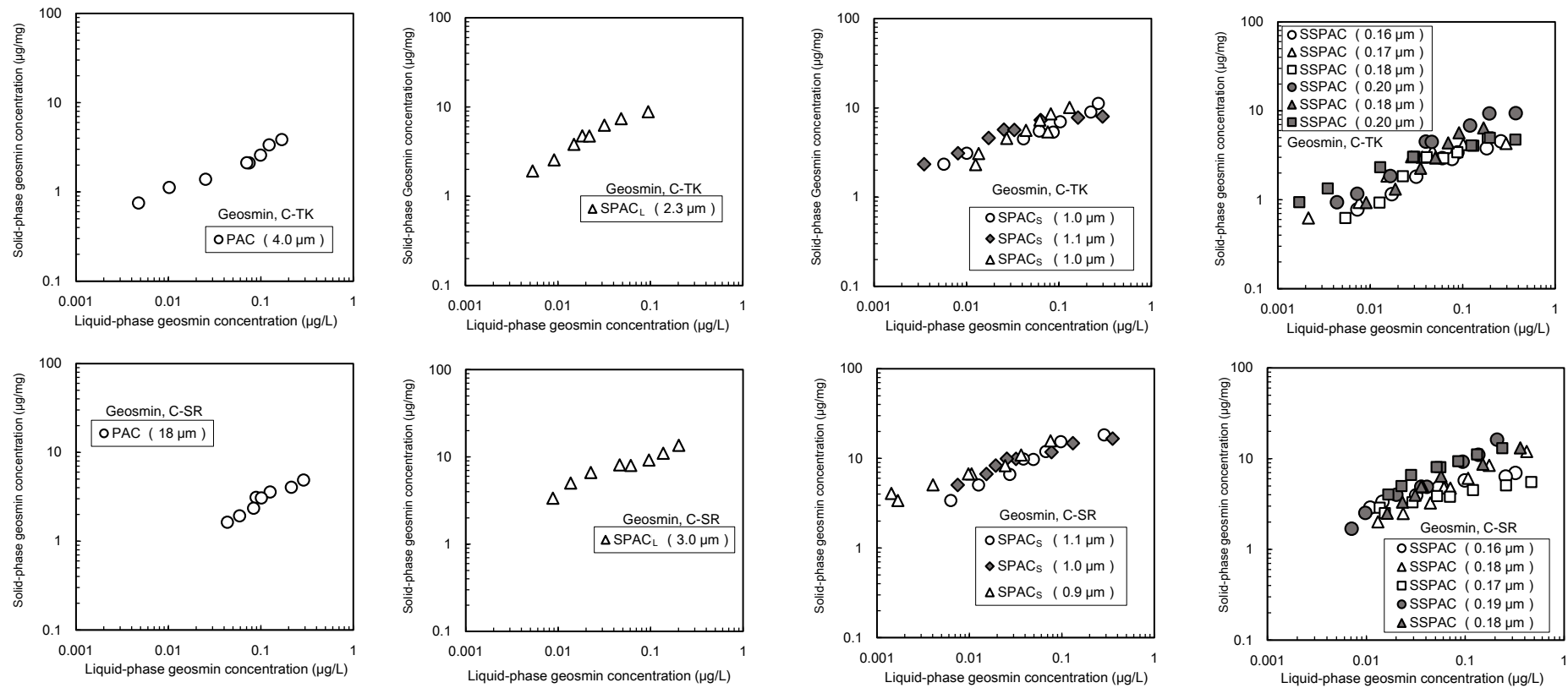


Fig 3S. Geosmin isotherms for C-TK and C-SR ACs of different particle sizes.

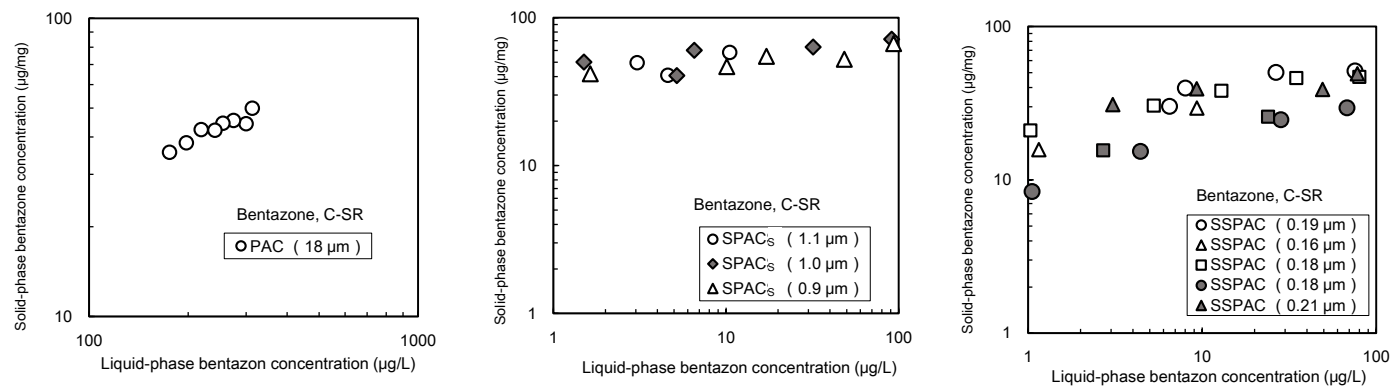


Fig 4S. Bentazone isotherms for C-SR ACs of different particle sizes.

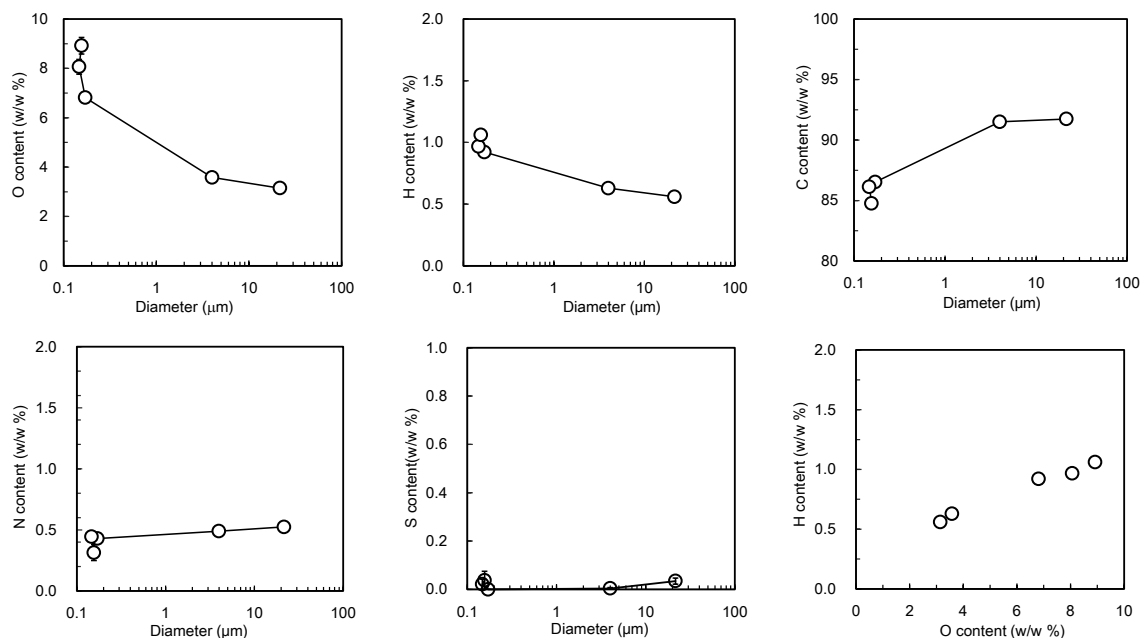


Figure 5S. Changes of O, H, C, N, and S content versus particle diameter during milling. The lower right panel is a plot of the relationship between O and H content. These are supplementary data to those presented in Figure 3. The elemental analysis was conducted just before the maintenance of the elemental analyzer, and so the absolute values might not be accurate. However, increases of O and H and a decrease of C were observed. The carbon was W-TK.

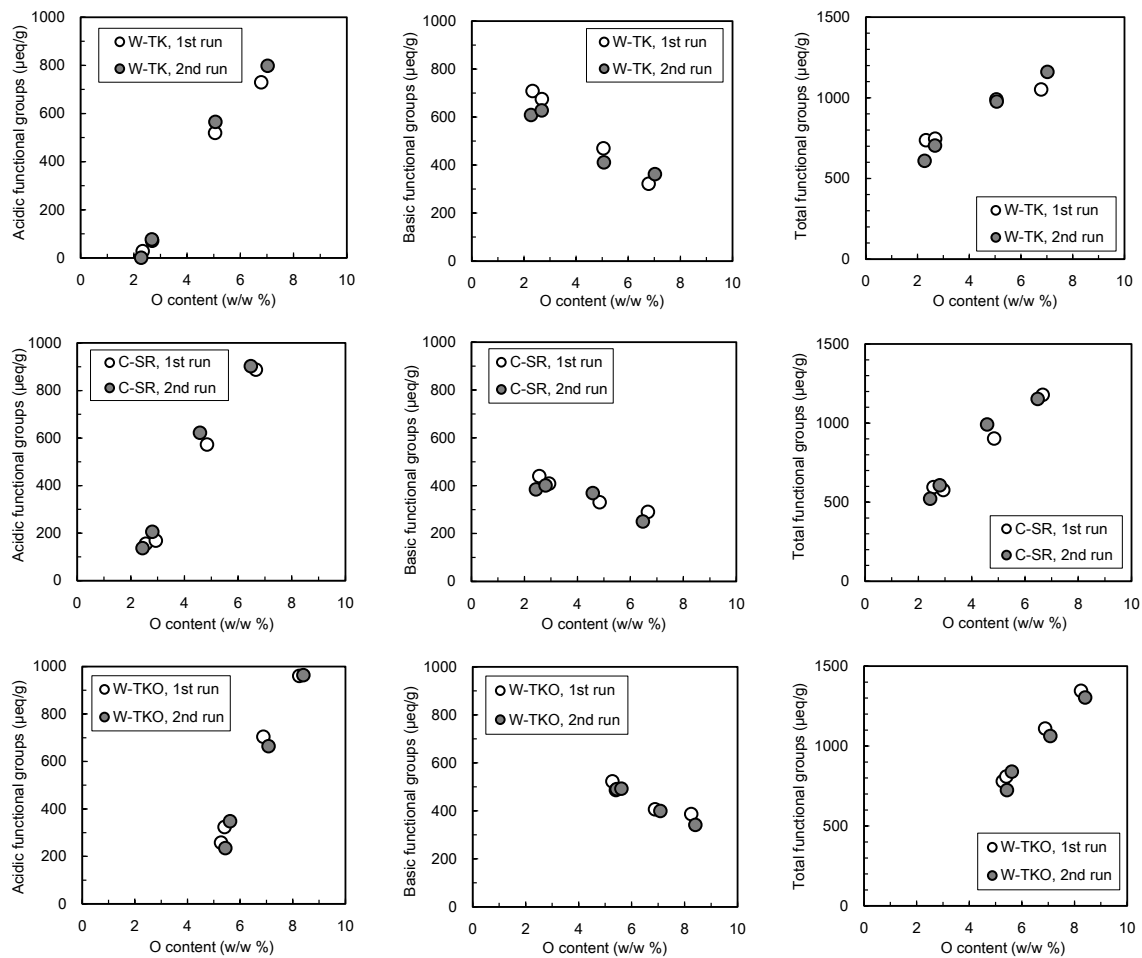


Figure 6S. Amount of acidic and basic functional groups and total amount of functional groups, as determined by Boehm titration, versus oxygen content during milling.

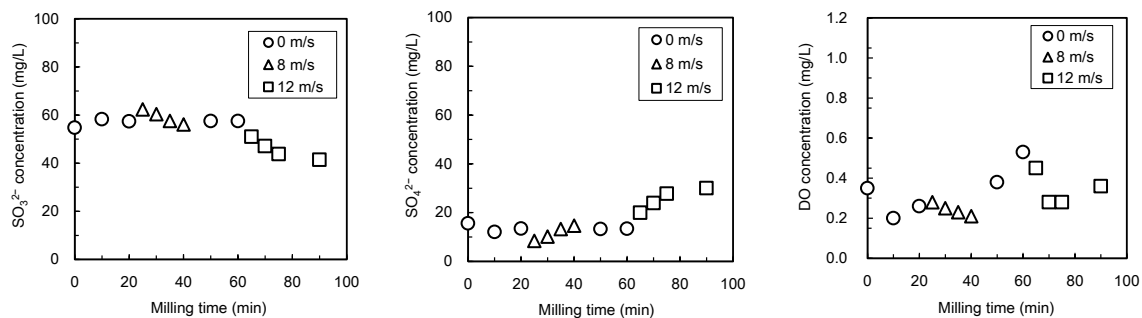


Figure 7S. Sulfate ion, sulfite ion, and DO concentrations during milling. Milling speed was changed from 0 m/s to 8 m/s at 20 min, to 0 m/s at 40 min, and to 12 m/s at 60 min. Milling was conducted without AC because the carbon would affect the sulfate and sulfite ion concentrations because of its ion exchange ability.

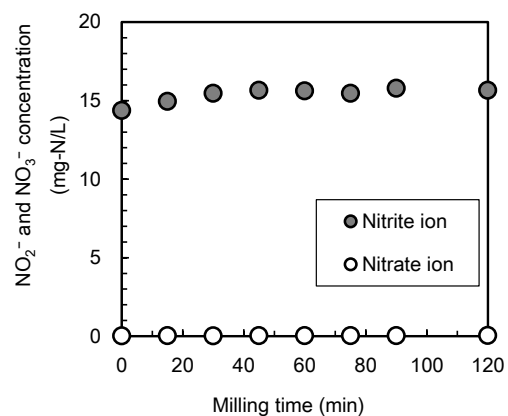


Figure 8S. Nitrite and nitrate concentrations during milling. Milling speed was 8 m/s. Milling was conducted without AC because the carbon would affect the nitrite and nitrate ion concentrations because of its ion exchange ability.

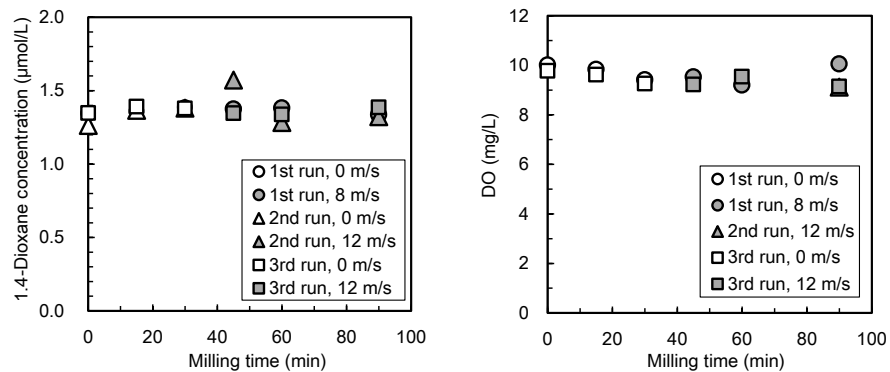


Figure 9S. 1,4-Dioxane concentration and DO concentration during milling. Milling speed was changed from 0 m/s to 8 or 12 m/s at 30 min. Milling was conducted without AC because the carbon would change the 1,4-dioxane concentration because of its adsorption ability.

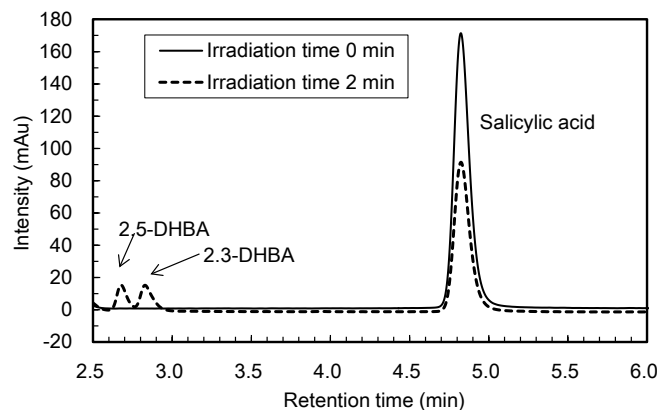


Figure 10S. Chromatograms of salicylic acid solution during vacuum-ultraviolet irradiation. Initial salicylic acid concentration, 10 mg/L; irradiation intensity, 1.3 mW/cm². Experiments were conducted without AC because the carbon would change the salicylic acid concentration because of its strong adsorption ability.

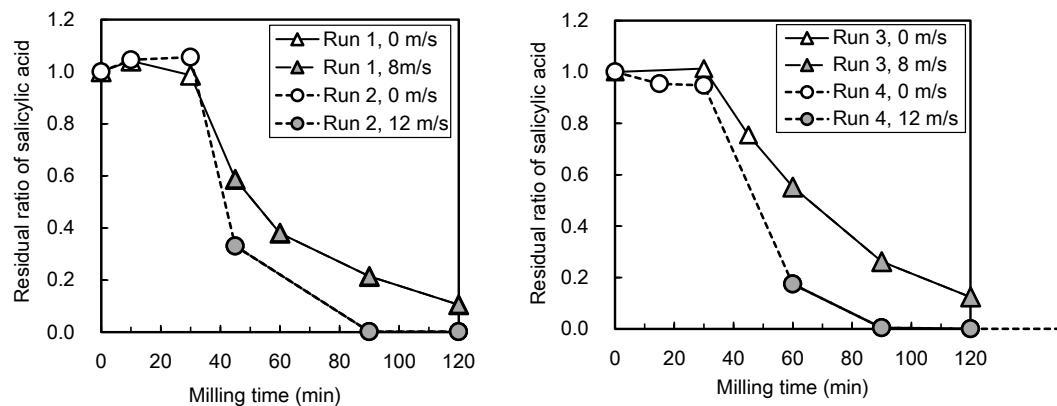


Figure 11S. Salicylic acid concentration during milling. Initial salicylic acid concentration, 1.7 (left) and 10 mg/L (right). Milling was conducted without AC because the carbon would change the salicylic acid concentration because of its strong adsorption ability.

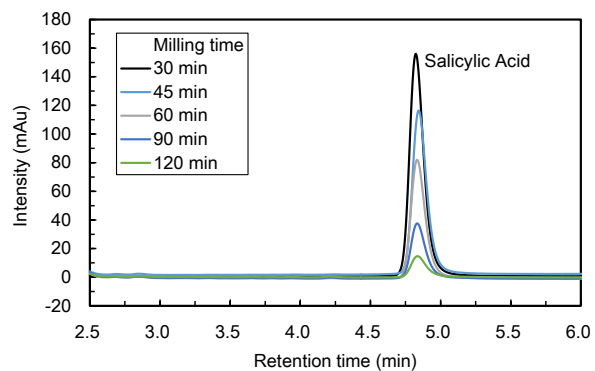


Figure 12S. Chromatograms of salicylic acid solution during milling. Milling speed, 8 m/s; initial salicylic acid concentration, 10 mg/L. Milling was conducted without AC because the carbon would change the salicylic acid concentration because of its strong adsorption ability.

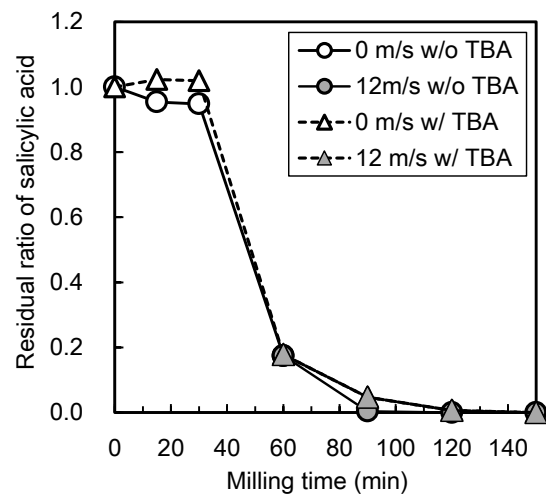


Figure 13S. Effect of tertiary butanol (TBA) on the decomposition of salicylic acid during milling. Initial salicylic acid and TBA concentrations were 10 and 1 mg/L, respectively. Milling was conducted without AC because the carbon would change the salicylic acid and TBA concentrations because of its strong adsorption ability.

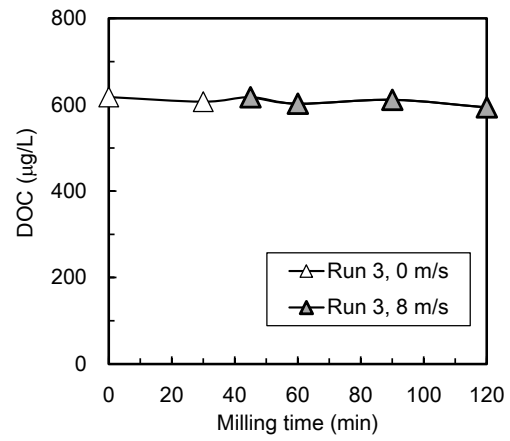


Figure 14S. Dissolved organic carbon concentration in salicylic acid solution during milling. Initial salicylic acid concentration, 1.7 mg/L. Milling was conducted without AC because the carbon would change the salicylic acid concentration because of its strong adsorption ability.

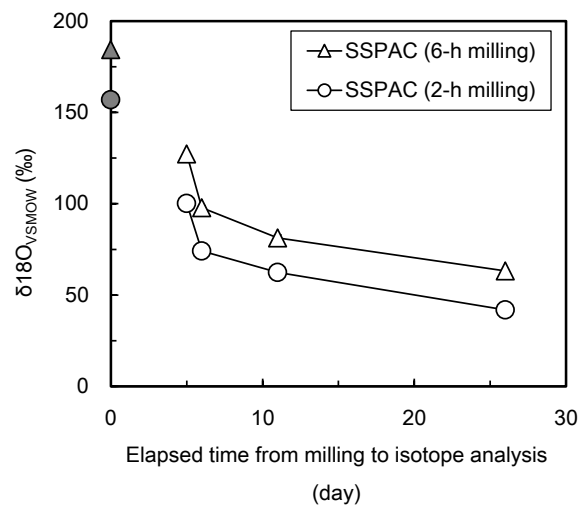


Figure 15S. Change of $^{18}\text{O}/^{16}\text{O}$ ratio between milling and isotope analysis. Open plots show experimental data. Closed plots show predicted values obtained by taking the mass balance of the oxygen content under the assumption that the additional oxygen atoms in the SSPAC after the milling originated entirely from the surrounding water and were characterized by an $^{18}\text{O}/^{16}\text{O}$ ratio identical to that of the surrounding water. The carbon was W-TK.

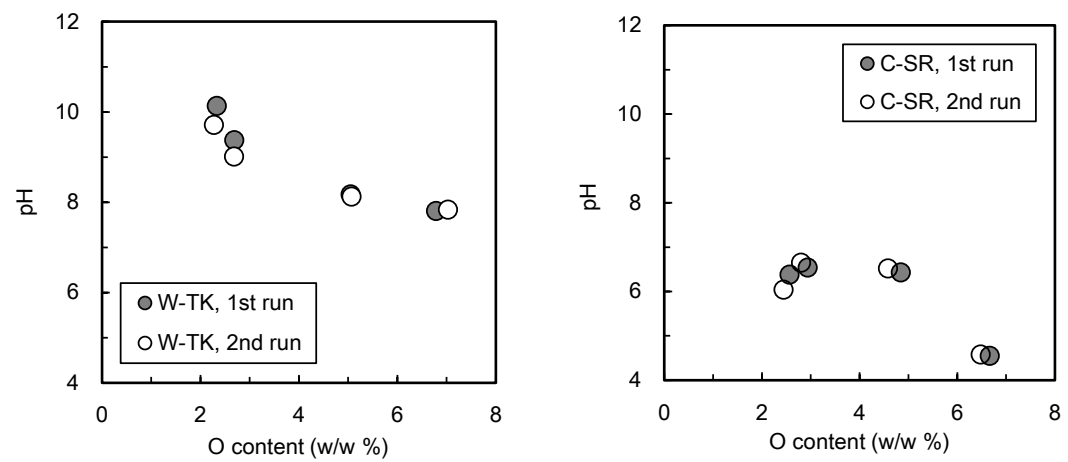


Figure 16S. pH of activated carbon slurry versus O content during milling.

References

- Adams, C.D., et al. (1994) Oxidation and Biodegradability Enhancement of 1,4-Dioxane Using Hydrogen Peroxide and Ozone. *Environmental Science & Technology* 28(11), 1812-1818.
- Coleman, H.M., et al. (2007) Degradation of 1,4-dioxane in water using TiO₂ based photocatalytic and H₂O₂/UV processes. *Journal of Hazardous Materials* 146(3), 496-501.
- Domen, K., et al. (2000) Mechano-catalytic overall water-splitting into hydrogen and oxygen on some metal oxides. *Applied Energy* 67(1), 159-179.
- Hara, M., et al. (2000) A Study of Mechano-Catalysts for Overall Water Splitting. *The Journal of Physical Chemistry B* 104(4), 780-785.
- Hill, R.R., et al. (1997) Photocatalytic degradation of 1,4-dioxane in aqueous solution. *Journal of Photochemistry and Photobiology A: Chemistry* 108(1), 55-58.
- Jen, J.-F., et al. (1998) Determination of hydroxyl radicals in an advanced oxidation process with salicylic acid trapping and liquid chromatography. *Journal of Chromatography A* 796(2), 283-288.
- Karnik, B.S., et al. (2007) Use of Salicylic Acid as a Model Compound to Investigate Hydroxyl Radical Reaction in an Ozonation–Membrane Filtration Hybrid Process. *Environmental Engineering Science* 24(6), 852-860.
- Kazunari, D., et al. (2000) Photo- and Mechano-Catalytic Overall Water Splitting Reactions to Form Hydrogen and Oxygen on Heterogeneous Catalysts. *Bulletin of the Chemical Society of Japan* 73(6), 1307-1331.
- Klečka, G.M. and Gonsior, S.J. (1986) Removal of 1,4-dioxane from wastewater. *Journal of Hazardous Materials* 13(2), 161-168.
- Matsushita, T., et al. (2015) Decomposition of 1,4-dioxane by vacuum ultraviolet irradiation: Study of economic feasibility and by-product formation. *Process Safety and Environmental Protection* 94, 528-541.
- Oppenländer, T. (2007) Mercury-free sources of VUV/UV radiation: application of modern excimer lamps (excilamps) for water and air treatment. *Journal of Environmental Engineering and Science* 6(3), 253-264.
- Quan, X., et al. (2007) Generation of hydroxyl radical in aqueous solution by microwave energy using activated carbon as catalyst and its potential in removal of persistent organic substances. *Journal of Molecular Catalysis A: Chemical* 263(1), 216-222.
- Suh, J.H. and Mohseni, M. (2004) A study on the relationship between biodegradability enhancement and oxidation of 1,4-dioxane using ozone and hydrogen peroxide. *Water Research* 38(10), 2596-2604.
- Tabatabaei, A.R. and Abbott, F.S. (1999) LC/MS analysis of hydroxylation products of salicylate as an indicator of in vivo oxidative stress. *Free Radical Biology and Medicine* 26(7), 1054-1058.